Title: Localisation and interactions between Arabidopsis auxin biosynthetic enzymes in the TAA/YUC-dependent pathway

Verena Kriechbaumer[1*], Stanley W. Botchway[2], Chris Hawes[1]

[1] Plant Cell Biology, Biological and Medical Sciences, Oxford Brookes University, Oxford OX3 0BP, United Kingdom

[2] Central Laser Facility, Science and Technology Facilities Council (STFC) Rutherford Appleton Laboratory, Research Complex at Harwell, Didcot OX11 0QX, United Kingdom

[*]**Correspondence**: Verena Kriechbaumer, vkriechbaumer@brookes.ac.uk

Plant Cell Biology, Biological and Medical Sciences, Oxford Brookes University, Oxford OX3 0BP, UK

Phone +44 (0)1865 483639

Fax: 44 (0)1865 483955

Email addresses:

vkriechbaumer@brookes.ac.uk, stan.botchway@stfc.ac.uk, chawes@brookes.ac.uk

Running title: Localisation of Arabidopsis auxin biosynthetic enzymes

Keywords: auxin biosynthesis, YUCCA, metabolon, *Arabidopsis thaliana*, localisation, protein-protein interaction, compartmentation, endoplasmic reticulum.

Highlight statement:

We show that a subset of enzymes in the Arabidopsis TAA/YUC route of auxin biosynthesis is localised to the endoplasmic reticulum and that microsomal fractions can produce auxin.

Word count total: 7698

Word count Summary: 142

Word count Introduction: 527

Word count Results: 1927

Word count Discussion: 1801

Word count Experimental procedures: 1433

Word count References: 2065

Word count Figure legends: 715

Summary

The growth regulator auxin is involved in all key developmental processes in plants. A complex network of a multiplicity of potential auxin biosynthetic pathways as well as transport, signalling plus conjugation and deconjugation lead to a complicated system of auxin function. This raises the question how such a complex and multifaceted system producing such a powerful and important molecule as auxin can be effectively organised and controlled. Here we report that a subset of auxin biosynthetic enzymes in the TAA/YUC route of auxin biosynthesis is localised to the endoplasmic reticulum (ER). ER microsomal fractions also contain a significant percentage of auxin biosynthetic activity. This could point toward a model of auxin function using ER membrane location and subcellular compartmentation for supplementary layers of regulation. Additionally we show specific protein-protein interactions between some of the enzymes in the TAA/YUC route of auxin biosynthesis.

Introduction

Auxin is the major plant growth hormone and responsible for important processes including photo- and gravitropism, senescence, responses to pathogens and abiotic stress (Sundberg and Østergaard, 2009; Llavata Peris *et al*., 2010; Scarpella *et al*., 2010; Zhao, 2010). At the cellular level auxin controls a broad variety of functions such as cell elongation, endocytosis and cell polarity (Perrot-Rechenmann, 2010, Grunewald and Friml, 2010).

Multiple pathways enhance the complexity of auxin biosynthesis. Parallel tryptophan-dependent and -independent pathways (Woodward and Bartel, 2005; Wang *et al*., 2015; Pieck *et al*., 2015; Kasahara 2015) act in different organs, developmental stages and environmental conditions (Normanly and Bartel, 1999; Östin *et al*., 1999). All these different routes can be independently and differentially regulated to build a metabolic network capable of dynamic changes to keep up auxin homeostasis or supply auxin maxima for local demands. Hence identifying the main or most dominant pathway of auxin biosynthesis and

combining data from various species is rather challenging and problematical (reviewed in Tivendale *et al*., 2014).

The TAA/YUC route in Arabidopsis auxin biosynthesis

As the first ever reported auxin depletion phenotype in Arabidopsis was published from knockouts of YUC genes, current research has concentrated on the TAA/YUC route of auxin biosynthesis. Multiple loss-of-function *yucca* mutations result in reduced IAA concentrations and defects in development, including plant height and fertility (Zhao *et al*., 2001; Cheng *et al*., 2006).The first step in auxin biosynthesis is catalysed by a protein family represented by *Weak Ethylene Insensitive8*(*Wei8*) / *Tryptophan Aminotransferase Of Arabidopsis 1* (*TAA1*). TAA1, TAR1 and TAR2 convert the amino acid tryptophan (Trp) to indole-3-pyruvic acid (IPyA) (Stepanova *et al*., 2008; Tao *et al*., 2008; Yamada *et al*., 2009; Zhou *et al*., 2011). TAA1 was shown to be responsible for rapid changes in IAA levels in shade avoidance and *taa1* mutants displayed reduced auxin levels (Tao *et al*., 2008). IPyA is then further converted to the auxin indole-3-acetic acid (IAA) by YUC proteins, a family of flavin-dependent monooxygenases. Interestingly even in a quadruple Arabidopsis *yucca* mutant the IAA levels are still 50% of WT levels (Stepanova *et al*., 2011). The TAA and YUC protein families jointly form a two-step biosynthetic route and constitute the main auxin biosynthesis pathway in *Arabidopsis* and maize (Mashiguchi *et al.*, 2011; Phillips *et al.*, 2011; Won *et al.*, 2011, Kriechbaumer *et al*., 2012; Kriechbaumer *et al*., 2015).

Subcellular location of auxin biosynthetic enzymes

We previously showed that the Arabidopsis *YUCCA* gene YUCCA4 exists in two major splice isoforms resulting in YUCCA4.2 featuring a C-terminal hydrophobic transmembrane domain (TMD) and therefore localising to the endoplasmic reticulum (ER) (Kriechbaumer *et al*., 2012). Additionally it was shown that in maize (*Zea mays*) roots and coleoptiles auxin biosynthetic activity can be found in microsomal fractions and at least three maize auxin biosynthetic proteins (*Zm*SPI1, *Zm*TAR1 and *Zm*TAR3) show ER-localisation (Kriechbaumer

55 *et al*., 2015). This could indicate a model of auxin function using ER membrane localisation
56 and subcellular compartmentation for additional layers of regulation and raises the question
57 about localisation of all the components of the Arabidopsis TAA/YUC route.
58 Here we report on the subcellular location of Arabidopsis TAA and YUC enzymes and *in vivo*
59 interactions between these enzymes.
60
61 **Results**
62 **Bioinformatics analysis of enzymes in the Arabidopsis TAA/YUC pathway**
63 *In silico* analysis of enzymes suggested being involved in the TAA/YUC route of Arabidopsis
64 auxin biosynthesis was carried out. This analysis predicted potential hydrophobic
65 transmembrane domains (TMD) for YUC3, YUC4.1, YUC5, and TAR2 (Table 1). According to
66 the algorithm TMHMM, YUC3 could feature an N-terminal TMD between the amino acid (aa)
67 31 and 53 for membrane insertion with the C-terminus facing the cytosol. YUC4.1 was shown
68 to possess a C-terminal TMD with the enzymatic N-terminus facing the cytosol
69 (Kriechbaumer *et al*., 2012). For YUC5 TMHMM predicts a TMD between aa 248 and 270
70 with the N-terminus resting in the cytosol (Table 1). TAR2 is suggested to have a TMD
71 between aa 7 and 26 with the N-terminal part of the enzyme facing the ER lumen.
72 Additionally using the prediction algorithm TargetP YUC5, YUC8, YUC9, YUC11, and TAR2
73 are indicated to possess an N-terminal signal anchor.
74
75 Another set of proteins in the TAA/YUC pathway of auxin biosynthesis (YUC1, YUC2,
76 YUC4.1, YUC6, YUC7, YUC10, TAA1, and TAR1) are predicted to be cytosolic and don`t
77 feature any hydrophobic domains. TMHMM indicates weak TMDs for YUC6 and YUC11 but
78 their probability calculations put them far below cut-off threshold (Table 1).
79
80 **Subcellular localisation of auxin biosynthetic enzymes**
81 The subcellular localisation of the proteins in the TAR/YUC auxin biosynthetic pathway in
82 Arabidopsis was tested using Agrobacterium-mediated transient expression in tobacco leaf

epidermal cells (Sparkes *et al*., 2006). Proteins of interest in this respect were, of course, enzymes with predicted TM domains and therefore with potential membrane localisations (Table 1). We have shown before that YUC4 exists in two splice variants with YUC4.1 being located in the cytoplasm, whereas YUC4.2 gains a C-terminal TMD in the splicing process and is therefore localised to the ER with its enzymatic N-terminal domain facing the cytoplasm (Kriechbaumer *et al*., 2012). Separately, TAA1 has been shown to be localised in the cytoplasm (Stepanova *et al*., 2008; Tao *et al*., 2008).

In the current study we have fused the remaining TAA/TAR and YUC proteins to N- or C-terminal fluorescent tags, respectively, so as not to interfere with the predicted TMDs. To determine their subcellular localisation these fusion proteins were co-expressed with the ER marker GFP-HDEL (Figure 1) and visualised by confocal microscopy. As predicted by their domain structure YUC3, YUC5, YUC8, YUC9, and TAR2 show colocalisation with the ER-marker GFP-HDEL (Figure 1). Interestingly also YUC7 shows ER-membrane localisation (Figure 1). YUC1, YUC2, YUC6, YUC11 and TAA1 are found in the cytosol (Figure 1).

To quantify the co-localization of the auxin constructs and the ER marker GFP-HDEL, Pearson's correlation coefficients (r) in the co-localized volume were determined using the ImageJ Pearson–Spearman correlation (PSC) colocalisation plug-in (French *et a*l., 2008). Values and representative scatter plots are shown in Supplementary Figure S1. In this analysis, r of 1 indicates a perfect correlation with the ER marker, and a value of 0 shows no correlation. As to be expected, the ER membrane proteins TAR2, YUC5, 7, 8, and 9 show correlation coefficients between 0.31 and 0.4. Cytosolic proteins have significantly lower r values in the range of 0.02 to 0.09 (Figure S1). As a proof-of concept we also overexpressed TAR2-mCherry in Arabidopsis in a stable manner and could confirm the ER localisation of TAR2 in Arabidopsis (Supplementary Figure S2).

As the auxin biosynthetic enzymes used in this study are tagged with fluorescent proteins it is important to show that the enzymes are still functional and correctly folded. For this we applied a novel leaf curling bioassay (Figure 2). Tobacco leaves expressing a combination of

a tagged TAA/TAR protein and a tagged-YUC protein show extensive leaf curling (Figure 2). This effect can be mimicked by injecting a 1 mM IAA solution in to the leaves. Interestingly expression of two TAA/TAR or two YUC constructs does not result in this leaf curling (Fig .2) indicating that both steps of the pathway are necessary to produce IAA amounts sufficient to produce the phenotype in tobacco leaves.

Auxin biosynthetic activity in Arabidopsis microsomes

Given the presence of at least six auxin biosynthetic enzymes on the ER membrane it was of interest to find out if auxin activity could also be found linked to the ER. For this ER microsome fractions were isolated from 5 days old Arabidopsis seedlings using a protocol modified from soybean and maize extractions (Abell *et al.*, 1997; Kriechbaumer *et al.*, 2015a).

To establish the purity of the microsomal fraction, immunoblots with three different antibodies were performed with cytosolic and microsomal fractions or total protein extract and microsomal fractions, respectively. The cytosolic and microsomal fractions were probed with antibodies raised against the cytosolic heat shock protein 70 (Hsp70, Figure 3). The microsomal fraction showed no detectable Hsp70 protein. To account for potential plasma membrane contamination, the total protein extract and the microsomal fraction and were blotted with anti-H^+ATPase antibodies recognizing the plasma membrane protein H^+ATPase in a variety of plants and fungi including Arabidopsis. An H^+ATPase band could be identified in the total protein extract but not in the microsomal fraction (Figure 3). Contamination of the microsomal fraction with mitochondria was investigated using antibodies against alternative oxidases (anti-AOX1/2). These quinol oxidases are located in the plant inner mitochondrial membrane. This mitochondrial marker could be detected in the total protein extract but not in the microsomal fraction (Figure 3).

Enzymatic tests using Trp or IPyA as a substrate were carried out using the microsomal fractions, the cytosolic supernatant as well as total Arabidopsis protein extract (Figure 4).

Boiled protein extracts from each fraction were used as negative controls to deduct unspecific IAA conversion from the enzymatic conversion in the assays. Assays were snap-frozen immediately after incubation time, IAA was extracted by ethyl acetate phase separation and quantified via HPLC and confirmed by GC-MS (Kriechbaumer *et al*., 2015a). Unspecific conversion was less than 5% of the enzymatic conversion rate for both substrates.

Auxin biosynthetic activity with the substrates Trp and IPyA was found both in microsomal as well as cytosolic fractions of Arabidopsis seedlings (Figure 4). The ER-linked conversion of Trp was about 18% of the total conversion for IPyA which was 25% (Figure 4).

Protein-protein interactions between auxin biosynthetic enzymes

The membrane association of auxin biosynthetic enzymes and ER-linked auxin activity raises the intriguing possibility that auxin biosynthesis might be compartmentalised. Additionally metabolic channelling in an "IAA synthase complex" has been postulated (Müller and Weiler, 2000). The formation of such metabolons characteristically comprises specific interactions between soluble enzymes that might be anchored to a membrane either by membrane-bound structural proteins that serve as nucleation sites for metabolon formation or by membrane-bound proteins involved in the pathway carried out by the metabolon. More evidence comes to light that pathways thought to contain only cytoplasmic enzymes are actually forming metabolons for subcellular structuring (reviewed in Jørgensen *et al*., 2005). Such a metabolon-based regulatory system could also explain how a single molecule like auxin can be effective in so many different developmental processes (Hawes *et al*., 2015).

To investigate the involvement of metabolic channelling, protein-protein interactions between TAA/TAR and YUC enzymes were investigated. To test for potential protein-protein interactions between auxin biosynthetic enzymes in the TAA/YUC pathway the methodology of FRET-FLIM was applied. Here the sensitivity and accuracy of Förster resonance energy transfer (FRET) to determine the colocalisation of two colour chromophores can now be improved to determine physical interactions by addition of fluorescence lifetime imaging

microscopy (FLIM). The technique allows measuring and determination of the space map of picoseconds fluorescence decay at each pixel of the image through confocal single and multiphoton excitation. FRET-FLIM measures the reduction in the excited state lifetime of the donor GFP fluorescence when an acceptor fluorophore (RFP) is within a distance of 1 to 10 nm, thus allowing FRET to occur and indicating a physical interaction between the two proteins of interest (Osterrieder *et al*., 2009; Sparkes *et al*., 2010; Schoberer and Botchway, 2014; Kriechbaumer *et al*., 2015). A reduction of as little as 200 ps in the excited-state lifetime of the GFP-labelled protein can represent quenching and indicates a protein-protein interaction (Stubbs *et al*., 2005). Due to limitations in the speed of photon counting of the FLIM apparatus, measurements were taken from the ER associated with the nuclear envelope as these areas of the ER are high-expressing with relatively low mobility. This enabled more reliable measurements than the fast-moving cortical ER (Sparkes *et al*., 2010; Kriechbaumer *et al*., 2015b).

Protein-protein interactions were first investigated using the ER-localised TAR2 protein as a donor (Figure 1, Table 2, Figure 5A) and both cytosolic as well as ER-localised YUC enzymes, respectively, as acceptors. Cytosolic YUC enzymes were included in this study as this method is sensitive enough to detect interactions between ER-anchored and cytosolic proteins at the interface between cytosol and ER (Kriechbaumer *et al*., 2015b) which is especially important in the context of metabolon formation between membrane-anchored and non-anchored but nonetheless interacting proteins. For this TAR2 fused to GFP was expressed transiently in tobacco epidermal leaf cells alone or together with YUC-proteins fused to mCherry. At least two biological samples with three different replicas each were used for statistical analysis.

TAR2-GFP alone showed a fluorescence lifetime of 3.1 ± 0.03 ns. Figure 5 shows the FRET-FLIM analysis for TAR2-GFP alone (Figure 5A-E, negative control) and for two interactions with YUC5-mCherry (Figure 5F-J) and YUC9-mCherry (Figure 5K-O), respectively. Raw FRET-FLIM images are shown in Figure 5A, F and K. The following analysis takes into account the lifetime values of each pixel within the region of interest which is visualized by a

pseudo-coloured lifetime map (Figure 5B, G and L). The graphs in Figure 5C, H and M show the distribution of these lifetimes within regions of interest with blue shades representing longer GFP fluorescence lifetimes than green ones. Decay curves (Figure 5D, I and N) of a representative single pixel highlight an optimal single exponential fit, where χ^2 values from 0.9 to 1.2 were considered an excellent fit to the data points (binning factor of 2 is applied). Confocal images showing the GFP construct in green and the mCherry construct in red are shown in Figure 5E, J and O.

This analysis example shows that most likely TAR2 and YUC5 interact as the lifetime values for the GFP/mCherry fusion pair (2.8 ± 0.03 ns; Table 2) are lower than those for TAR2-GFP alone (3.0 ± 0.05 ns). An interaction for TAR2 and YUC9 could not be determined as the lifetime for the fusion pair TAR2/YUC9 (3.0 ± 0.05 ns) is not statistically different from the lifetime of the negative control TAR2-GFP alone. Supplementary Figure S3 shows representative examples for FRET-FLIM data and the analysis steps for each combination tested (Figure S3).

Protein-protein interaction for TAR2 with other YUC proteins were tested and in this analysis TAR2 showed protein-protein interaction with YUC5 and YUC8 but not with YUC1, YUC2, YUC3, YUC6, YUC7, YUC9 and YUC11 (Table 2, Figures 6A and S3). Supplementary Figure S4 shows the colocalisation between TAR2 and YUC5 or YUC8, respectively (Figure S4).

Finally the protein-protein interaction between YUC-proteins was investigated (Table 2, Figure 6B and C and S3). As they interact with TAR2 and are ER-localised the enzymes YUC5 (Figure 6B) and YUC8 (Figure 6C) were chosen for this experiment. Both YUC5 and YUC8 showed interaction with a variety of YUC proteins tested: YUC5 with YUC5, YUC7, YUC9, and YUC11 (Figure 6B, S3 and Table 2) and YUC8 with YUC7 and YUC9 (Figure 6C, S3 and Table 2). Neither YUC5 nor YUC8 showed significant interaction with the cytosolic TAA1 protein.

Discussion

Localisation of auxin biosynthesis

Localisation studies of proteins involved in auxin function have long suggested the involvement of various sub-cellular compartments; auxin precursor pathways such as the shikimate and Trp biosynthetic pathways are suggested to be localised to plastids (Woodward and Bartel, 2005; Tzin and Gallili, 2010), whereas the further steps are believed to be localised in the cytosol (Woodward and Bartel, 2005; Mano and Nemoto, 2012; reviewed in Ljung, 2013). We have shown here that in transient overexpression in tobacco leaf epidermal cells a subset of auxin biosynthetic enzymes involved in the TAA/YUC route are localised to the ER membrane whilst others are cytosolic. With TAR2 and YUC4.2, 5, 7, 8, and 9 localised on the ER membrane and TAA1 and YUC1, 2, 3, 4.1, 6 and 11 in the cytoplasm (Figure 1; Kriechbaumer *et al*., 2012) we have a dual localisation for both steps in the TAA/YUC route of Arabidopsis auxin biosynthesis. We have shown a similar scenario before for *Zea mays* with *Zm*TAR1, *Zm*TAR3 and the YUC orthologue *Zm*SPI1 localised at the ER membrane and *Zm*VT2 and *Zm*YUC1 remaining cytoplasmic (Kriechbaumer *et al*., 2015a). Interestingly three of the ER-localised YUC proteins (YUC7, YUC8 and YUC9) together with the cytosolic YUC1 can suppress the dwarf phenotype of a weak brassinosteroid receptor mutant *bri1-301* (Kang *et al*., 2010). An auxin characteristic plant phenotype and overlapping expression pattern in the embryo have been shown in the quadruple mutant of yuc1/4/10/11 and YUC1, 2, 4, and 6 redundantly control venation in leaves and flowers (Cheng *et al*., 2006). It is noted that these YUC proteins are all cytosolic – with the yuc4 insertion not determining between the splice variants. It will be of great interest to create multiple mutants according to the localisation of proteins to evaluate the contribution of membrane anchoring to auxin biosynthetic capacity.

Additionally, in both Arabidopsis seedlings (Figure 4) and maize primary roots and coleoptiles (Kriechbaumer *et al*., 2015a) a significant percentage of auxin biosynthetic activity can be found in the microsomal fraction which mainly consists of ER. This activity together

with the localisation of enzymes involved raises the intriguing possibility of an additional level of regulation of biosynthesis and potentially also storage of compounds in different subcellular compartments. Trp is involved in a variety of other pathways such as the biosynthesis of proteins and defence compounds and also the size of the Trp pool is about 40 times larger than the pool of IAA and 25 times larger than for IPyA (Novák *et al*., 2012). This highlights the need for compartmentalisation of precursors and/or enzymes involved as well as pathway regulation to avoid overproduction of the highly active IAA molecules (Sairanen *et al*., 2012). Fluorescent auxin analogues that do not display auxin activity *in planta* but have been shown to mimic transport of endogenous IAA are also mainly localized to the endoplasmic reticulum in cultured cells and roots, indicating the possibility of a subcellular compartmentalised auxin gradient in the cells (Hayashi *et al*., 2014).

Recent data also indicate a regulatory role for the transport into the ER via specific PIN and PILS proteins; localization studies revealed that PIN5, PIN6, and PIN8 mainly localize to the ER (Mravec *et al*., 2009; Dal Bosco *et al*., 2012; Ding *et al*., 2012; Bender *et al*., 2013; Sawchuk *et al*., 2013) but PIN5 and PIN8 could also be detected on the plasma membrane (Ganguly *et al*., 2014). Hereby PIN5 and PILS2 and PILS5 are capable of enhancing auxin compartmentation between ER and cytosol whereas the pollen-specific PIN8 protein is suggested to act antagonistically and decrease compartmentation (Mravec *et al*., 2009; Barbez *et al*., 2012). Overexpression of the ER-localised PIN5 results in a decrease of free IAA and increased levels of conjugated IAA possibly suggesting additional levels of auxin regulation in the ER lumen (Mravec *et al*., 2009). It is suggested that ER-localised PINs function in regulating auxin homeostasis via subcellular auxin compartmentalization, as auxin transported into ER lumen is inaccessible for nuclear signaling (Mravec *et al*., 2009). In the ER auxin can then be inactivated by ER-localized auxin conjugating enzymes (Mravec *et al*., 2009) for instance several IAA-amino acid conjugate hydrolases have been shown to be located at the ER (Woodward and Bartel, 2005).

Protein interactions between auxin biosynthetic enzymes raising the possibility of a metabolon?

Precursor channelling via an IAA synthase complex has been suggested as many enzymes potentially involved in auxin biosynthesis have low substrate specificities and turnover rates (Pollmann *et al*., 2009). The existence of an auxin biosynthetic metabolon (Müller and Weiler, 2000; Kriechbaumer *et al*., 2006) a functional multienzyme complex tethered together by non-covalent binding typically receiving stabilization from membrane or cytoskeletal anchoring, is also a suggested possibility. Such multi-enzyme complexes have been shown for the Calvin-Benson cycle (Graciet *et al*., 2004), Arabidopsis dhurrin (Nielsen *et al*., 2008; Jensen *et al*., 2011) and sporopollenin biosynthetic pathways (Lallemand *et al*., 2013) and recently the isoflavonoid pathway in soybean (Dastmalchi *et al*., 2016). Metabolons allow for direct transport of the product from an enzymatic reaction to act as a substrate for the next enzymatic step thereby enhancing substrate concentrations and turnover rates and protection for unstable or toxic intermediates (Srere, 1985; Ralston and Yu, 2006; Møller, 2010; reviewed in Hawes *et al*., 2015). For example the intermediate IPyA is highly unstable when dissolved in water and converts to IAA; this is far less the case if IPyA is dissolved in alcohols such as methanol or in plant extracts. Additionally many enzymes suggested to be involved in auxin biosynthesis have low substrate specificities and turnover rates. To exemplify turnover rates, for YUC6 the k_{cat} for oxidation of NADPH was shown to be 0.31 s^{-1} (Dai *et al*., 2013) whereas RuBisCO which is considered to have a low turnover rate has a k_{cat} of~3 s^{-1} (Sage, 2002). To compensate for the low turnover kinetics of these enzymes an auxin metabolon has been postulated (Müller and Weiler, 2000). However, purification attempts (Müller and Weiler, 2000; Kriechbaumer *et al*., 2006) and yeast-2-hybrid approaches have not identified the proteins involved in auxin biosynthesis. A possible explanation is that IAA biosynthesis occurs at membrane surfaces catalysed by membrane anchored enzymes such as YUCCA4.2 or metabolons, which would impede the detection by such approaches due to their membrane binding or nuclear mislocalisation in the conventional yeast-2-hybrid, respectively. Such a metabolon-based regulatory system could

306 also explain how a single molecule like auxin can be effective and strictly controlled in so
307 many different developmental processes. The ER-membrane localised proteins YUC4.2
308 (Kriechbaumer *et al*., 2012) and YUC5, YUC7, YUC8, YUC9, and TAR2 could well work as
309 scaffolding protein for such a metabolon complex also allowing for other cytosolic TAA/YUC
310 enzymes to be part of the complex by protein-protein interactions.
311
312 The FRET-FLIM interactions between TAR2 and YUC5 and YUC8 (Figure 6A), respectively,
313 as well as the interactions between YUC5 (Figure 6B) and YUC8 (Figure 6C) with other YUC
314 proteins could potentially be the building blocks of larger protein complexes aiding further
315 regulatory mechanisms. This protein complex can be composed of membrane-bound and
316 cytosolic enzymes together with scaffolding and regulatory proteins such as P450 enzymes
317 or chaperone proteins. This raises the question why seemingly in a very specific manner
318 YUC5 and YUC8 interact with TAR2 but not the other ER-localised proteins YUC7 or YUC9
319 or even cytosolic YUC proteins (Figure 6A)? YUC5 was first described in the *super1-D*
320 mutant that acts as a suppressor of the partial loss-of-function mutant allele *er-103* of the
321 ERECTA gene (Woodward *et al*., 2005b). ERECTA is involved in inflorescence architecture
322 (Torii *et al*., 1996) and overexpression of YUC5 results in elevated free auxin levels and
323 characteristic phenotypes such as increased hypocotyl length and narrow leaves (Woodward
324 *et al*., 2005b). It was concluded that auxin biosynthesis via YUC5 and the ERECTA pathway
325 work independently but with potential overlaps in determining inflorescence architecture via
326 cell division and cell expansion (Woodward *et al*., 2005b). YUC5 is mainly expressed in roots
327 and young vegetative tissue but not in flowers and during the inflorescence developmental
328 stage (Woodward *et al*., 2005b).
329 YUC8 *was recently* linked to jasmonic acid (Hentrich *et al*., 2013a) and ethylene signalling
330 (Hentrich *et al*., 2013b) and is furthermore regulated by temperature via the phytochrome-
331 interacting factor 4 (PIF4; Sun *et al*., 2012). Both YUC5 and YUC8 together with YUC2 and
332 YUC9 are transcriptionally up-regulated when plants are under shade, also correlating with
333 an increase in free auxin levels (Xie *et al*., 2015); the transcription factor KANADI1 is capable

of transcriptional repression of YUC2, YUC5 and YUC8 and can therefore inhibit shade-induced auxin biosynthesis (Xie *et al*., 2015). Furthermore both YUC5 and YUC8 again interact with a different subset of the YUC proteins tested: YUC5 homodimerizes with YUC5 and interacts with the ER-localised YUC7 and YUC9 as well as with the cytosolic protein YUC11 (Figure 6B); YUC8 shows interaction with the drought-induced YUC7 and homodimerizes with YUC8 itself (Figure 6C). Further investigation of these interactions as well as proteomic immunoprecipitation studies will aim to reveal the composition and dynamics of such a protein complex.

Auxin biosynthesis responds to a plethora of environmental factors and therefore has to be rather versatile. It has recently been shown to relate for example, to sugar signalling; via the Phytochrome Interacting Factor (PIF) transcription factors soluble sugars can upregulate IAA biosynthesis in Arabidopsis (Sairanen *et al*., 2012; Lilley *et al*., 2012) and sugars have also been shown to influence auxin biosynthesis in developing maize kernels (LeClere *et al*., 2010). Another factor is light: IAA biosynthesis via the TAA1/YUC pathway is stimulated in response to changes in the ratio of red to far-red light in shade conditions (Tao *et al*., 2008). Also this response is under the regulation of PIF genes (Hornitschek *et al*., 2012). *PIF*-mediated regulation has also been shown for *TAA1 a*nd *YUC8* in temperature regulation of IAA biosynthesis (Franklin *et al*., 2011; Sun *et al*., 2012). It is intriguing that all these different responses are regulated by PIF transcription factors. The potential of a metabolon with changing compositions and/or numbers of TAA/TAR and YUC proteins would provide additional regulatory power under changing environmental and developmental situations.

ER lipid subdomains have been described to be capable of supporting metabolon assembly (Zajchowski and Robbins, 2002) and metabolon localisation on the ER could potentially also add an aspect of mobility as the ER surfaces has been shown to be mobile (Runions *et al*. 2006). For instance, ER micro-domains could move metabolons around in an actin-guided way if under pathogen attack (Chuong *et al*., 2004). It is a possibility that metabolon formation allows production of the basic structures and depending on developmental stage,

362 tissue or stress situation additional or different enzymes could be recruited to the metabolons
363 for specific structural changes, such as in output or to supply additional regulatory aspects
364 during production (Jørgensen *et al*., 2005).

Experimental procedures

Cloning of expression plasmids

Primers were obtained from Eurofins Genomics. Q5 high-fidelity DNA polymerase (New England Biolabs) was used for all polymerase chain reaction reactions. Genes of interest were cloned into the modified binary vector pB7WGF2 containing an N- or pB7FWG containing a C-terminal GFP fluorescent proteins (Karimi *et al*., 2005) using Gateway technology (Invitrogen).

Plant material and transient expression in tobacco epidermal leaf cells

For Agrobacterium-mediated transient expression, 5-week-old tobacco (*Nicotiana tabacum* SR1 cv Petit Havana) plants grown in the greenhouse were used. Transient expression was carried out according to Sparkes *et al*. (2006). In brief, each expression vector was introduced into Agrobacterium strain GV3101 by heat shock. Transformants were inoculated into 5 ml of YEB medium (per litre: 5 g of beef extract, 1 g of yeast extract, 5 g of sucrose and 0.5 g of $MgSO_4 \cdot 7H_2O$) with 50 µg/ml spectinomycin and rifampicin. After overnight shaking at 25°C, 1 ml of the bacterial culture was pelleted by centrifugation at 2,200 × g for 5 min at room temperature. The pellet was washed twice with 1 ml of infiltration buffer (50 mM MES, 2 mM $Na_3PO4.12H_2O$, 0.1 mM acetosyringone and 5 mg/ml glucose) and then resuspended in 1 ml of infiltration buffer. The bacterial suspension was diluted to a final OD_{600} of 0.1 and carefully pressed through the stomata on the lower epidermal surface using a 1 ml syringe. Transformed plants then were incubated under normal growth conditions for 48 h. Images were taken using a Zeiss 880 laser scanning confocal microscope with 63x oil immersion objective. For imaging of the GFP/RFP combinations, samples were excited using 488 and 543 nm laser lines in multi-track mode with line switching. Images were edited using the ZEN image browser.

Leaf curling bioassay

For the leaf curling assay to assess induced auxin biosynthesis, tobacco plants were infiltrated with TAA, TAR and YUC constructs in varying combinations as described above. 1 mM IAA dissolved in infiltration buffer was infiltrated into the leaf epidermal cells the same way. Plants were kept in growth chambers for 48h before images were taken. Expression was checked using confocal microscopy as described above.

FRET-FLIM data acquisition

Epidermal samples of tobacco leaves infiltrated as described above were excised and the GFP and mRFP expression levels in the plant within the region of interest were confirmed using a Nikon EC2 confocal microscope with excitation at 488 and 543 nm, respectively. FRET-FLIM data capture was performed according to Osterrieder *et al*. (2009) and Kriechbaumer *et al.* (2015b) using a two-photon microscope at the Central Laser Facility of the Rutherford Appleton Laboratory.

In brief, a two-photon microscope built around a Nikon TE2000-U inverted microscope was used with a modified Nikon EC2 confocal scanning microscope to allow for multiphoton FLIM (Botchway *et al*., 2015). 920 nm laser light was produced by a mode-locked titanium sapphire laser (Mira; Coherent Lasers), producing 200-fs pulses at 76 MHz, pumped by a solid-state continuous wave 532-nm laser (Verdi V18; Coherent Laser). The laser beam was focused to a diffraction limited spot through a water-immersion objective (Nikon VC; 360, numerical aperture of 1.2) to illuminate specimens on the microscope stage. Fluorescence emission was collected without descanning, bypassing the scanning system, and passed through a BG39 (Comar) filter to block the near-infrared laser light. Line, frame, and pixel clock signals were generated and synchronized with an external detector in the form of a fast microchannel plate photomultiplier tube (Hamamatsu R3809U). Linking these via a time-correlated single-photoncounting PC module SPC830 (Becker and Hickl) generated the raw FLIM data.

Data were analyzed by obtaining excited-state lifetime values of a region of interest on the nucleus, and calculations were made using SPC Image analysis software version 5.1

(Becker and Hickl). The distribution of lifetime values within the region of interest was generated and displayed as a curve. Only values that had a χ^2 between 0.9 and 1.4 were taken. The median lifetime value and minimum and maximum values for one-quarter of the median lifetime values from the curve were taken to generate the range of lifetimes per sample. At least three nuclei from at least two independent biological samples per protein-protein combination were analyzed, and the average of the ranges was taken.

ER microsome preparation

All following steps were performed on ice or 4^{o}C unless indicated otherwise. 5 g of Arabidopsis seedlings (5 days after germination) were ground in liquid nitrogen using a mortar and pestle. The resulting powder was homogenised in approximately 4 ml of buffer A (25 mM TEA-HOAc pH7.5, 50 mM KOAc pH7.5, 5 mM $Mg(OAc)_2$, 0.25 M sucrose, 4 mM DTT). Then 4 ml of buffer B (100 mM TEA-HOAc pH7.5, 20 mM EDTA) were added and the suspension was incubated on ice for 10 min. After centrifugation at 1,000 g for 10 min the resulting supernatant was poured over 2 layers of cheese cloth into a fresh tube. That extract was centrifuged again at 4,500 g for 25 min. In ultracentrifuge tubes the 8 ml suspension were layered on 4 ml of sucrose cushion (Buffer C: 25 mM TEA-HOAc pH7.5, 25 mM KOAc pH7.5, 2 mM $Mg(OAc)_2$, 0.5 M sucrose, 4 mM DTT). Using the swing-out rotor SW41 this was spun for 90 min at 93,000 g. The resulting pellet was resuspended in 200 µl buffer D (25 mM TEA-HOAc pH7.5, 0.25M sucrose, 1 mM DTT) using a glass rod and a 2 ml Potter-Elvehjem homogeniser. Freshly prepared microsomes were used for enzymatic assays straight away.

IAA quantification

Enzymatic activity tests with microsomal and cytosolic fractions were carried out in 100 mM TRIS-HCl, pH 8.0, using 20 µl of plant extract, 1 mM NADPH, 100 µM FAD, and 100 µM tryptophan or IPA in a total volume of 100 µl. As an internal standard, for further GC_MS analysis 2,4,5,6,7-pentadeuteriated IAA (Cambridge Isotope Laboratories, UK) was included.

After incubation for 1 h in a 37 ºC water bath, the assays were snap-frozen in liquid nitrogen and IAA extracted by ethyl acetate phase separation (Park *et al.*, 2003; Kriechbaumer *et al.*, 2007).

In brief, the pH of the sample was increased over 9.5 with 1 M Na_2CO_3 and the then extracted with 400 µl of ethyl acetate. The aqueous lower phase was recovered, 200 µl of water were added, the partitioning procedure was repeated, and again the aqueous phase was recovered and combined with the aqueous phase from the previous partitioning step. The collected aqueous phase was acidified with acetic acid to a pH below 2.5 and partitioned twice with addition of 400 µl of ethyl acetate for each step. This time the organic phases were collected and the liquid evaporated using a speed-vac (Centrivap, Labconco). The dried pellets were re-dissolved in 100% methanol and analysed via high-performance liquid chromatography (HPLC) with a reverse phase column (Apollo C18, 250 mm×4.6 mm, 5 µm, Grace). IAA was quantified via a HPLC system (Waters 600E) in isocratic flow of 0.8 ml min–1 with a 40:60 mixture of buffer A (10% methanol, 0.3% acetate) and buffer B (90% methanol, 0.3% acetate). Peaks were identified by comparison with the standard substances with respect to retention time and UV spectrum using both a UV monitor (Waters 486) and a fluorescence monitor (Waters 470).

To confirm and quantify IAA GC-MS was applied (Kriechbaumer et al., 2015a). In brief: IAA-containing HPLC fractions were collected, and dried and dissolved in 20 µl of methanol. For derivatization 50 µl of ethereal diazomethane (Sigma-Aldrich) were added to each sample and incubated for 30 min in a fume hood. Tubes were set to dried under vacuum for 10 min and any remaining solution in the tubes was blown off with pure N2 gas. The derivatized samples were dissolved in 10 µl of pure methanol and 1 µl of the solution was injected to gas chromatography–mass spectrometry (GC-MS; CP-3800, Saturn 2200, Varian) in the split-less mode. The identity of derivatized IAA was confirmed by 130 and 189 fragmentation ions and normalized against the internal standard recognized by 135 and 184 fragmentation ions. The signals in the peak area of the 130 fragmentation ion were quantified using external standards.

476

477 **Western blotting of total protein extract, microsomal and cytosolic fractions**

478 100 µg protein of total protein extract, the cytosolic and microsomal fractions, respectively,
479 was separated on a 12% (v/v) SDS–polyacrylamide gel, transferred to a nitrocellulose
480 membrane, and probed with antiHsp70 antibodies (1:1000, Agrisera), anti-H+ATPase
481 antibodies (1:1000, Agrisera), or anti-AOX1/2 antibodies (1:1000, Agrisera), respectively.
482 The membrane was further incubated with anti-rabbit immunoglobulin G conjugated with
483 Cy5, and the signal was detected with a fluorescence scanner using a red fluorescence filter.

484

485 **Acknowledgements**

486 The authors thank Dr Joseph McKenna for the gift of the mCherry-vector.

487 This work was supported by the Science and Technology Facilities Council Program (grant
488 no. 14230008) awarded to CH.

References

Abell BM, Holbrook LA, Abenes M, Murphy DJ, Hills MJ, Moloney MM. 1997. Role of the proline knot motif in oleosin endoplasmic reticulum topology and oil body targeting. Plant Cell **9**, 1481–1493.

Barbez E, Kubes M, Rolcik J, Beziat C, Pencik A, Wang B, Rosquete M.R, Zhu J, Dobrev PI, Lee Y, Zažímalovà E, Petrášek J, Geisler M, Friml J, Kleine-Vehn J. 2012. A novel putative auxin carrier family regulates intracellular auxin homeostasis in plants. Nature **485**, 119–122.

Bender RL, Fekete ML, Klinkenberg PM, Hampton M, Bauer B, Malecha M, Lindgren K, A Maki J, Perera MA, Nikolau BJ, Carter CJ. 2013. PIN6 is required for nectary auxin response and short stamen development. Plant Journal **74**, 893–904.

Botchway SW, Scherer KM, Hook S, Stubbs CD, Weston E, Bisby RH, Parker AW 2015. A series of flexible design adaptations to the Nikon E-C1 and E-C2 confocal microscope systems for UV, multiphoton and FLIM imaging. Journal of Microscopy **258**, 68–78.

Cheng Y, Dai X, Zhao Y. 2006. Auxin biosynthesis by the YUCCA flavin monooxygenases controls the formation of floral organs and vascular tissues in Arabidopsis. Genes & Development **20**, 1790–1799.

Chuong SDX, Good AG, Taylor GJ, Freeman MC, Moorhead GBG, Muench DG. 2004. Large-scale identification of tubulin-binding proteins provides insight on subcellular trafficking, metabolic channelling and signalling in plant cells. Molecular & Cellular Proteomics **3**, 970–983.

Dai X, Mashiguchi K, Chen Q, Kasahara H, Kamiya Y, Ojha S, DuBois J, Ballou D, Zhao Y. 2013. The biochemical mechanism of auxin biosynthesis by an Arabidopsis YUCCA flavin-containing monooxygenase. Journal of Biological Chemistry **288**, 1448–1457.

Dal Bosco CD, Dovzhenko A, Liu X, Woerner N, Rensch T, Eismann M, Eimer S, Hegermann J, Paponov IA, Ruperti B, Heberle-Bors E, Touraev A, Cohen JD, Palme K. 2012. The endoplasmic reticulum localized PIN8 is a pollen-specific auxin carrier involved in intracellular auxin homeostasis. Plant Journal **71**, 860–870.

Dastmalchi M, Bernards M, Dhaubhadel S. 2016. Twin anchors of the soybean isoflavonoid metabolon: evidence for tethering of the complex to the endoplasmic reticulum by IFS and C4H. Plant Journal doi: 10.1111/tpj.13137.

Ding Z, Wang B, Moreno I, Dupláková N, Simon S, Carraro N, Reemmer J, Pěnčík A, Chen X, Tejos R, Skůpa P, Pollmann S, Mravec J, Petrášek J, Zažímalová E, Honys D, Rolčík J, Murphy A, Orellana A, Geisler M, Friml J. 2013. ER-localized **auxin** transporter PIN8 regulates **auxin** homeostasis and male gametophyte development in Arabidopsis. Nature Communication **3**, 941.

David KM, Couch D, Braun N, Brown S, Grosclaude J, Perrot-Rechenmann C. 2007. The auxin-binding protein 1 is essential for the control of cell cycle. Plant Journal **50**, 197–206.

Franklin KA, Lee SH, Patel D, Kumar SV, Spartz AK, Gu C, Ye S, Yu P, Breen G, Cohen JD *et al*. 2011. Phytochrome-interacting factor 4 (PIF4) regulates auxin biosynthesis at high temperature. Proceedings of the National Academy of Sciences **108**, 20231–20235.

French AP, Mills S, Swarup R, Bennett1 MJ, Pridmore TP. 2008. Colocalization of fluorescent markers in confocal microscope images of plant cells. Nature Protocols **3**, 619–628.

Ganguly A, Park M, Kesawat MS, Cho HT. 2014. Functional analysis of the hydrophilic loop in intracellular trafficking of Arabidopsis PIN-FORMED proteins. Plant Cell **26,** 1570–1585.

Graciet E, Lebreton S, Gontero B. 2004. Emergence of new regulatory mechanisms in the Benson-Calvin pathway via protein-protein interactions: a glyceraldehyde-3-phosphate dehydrogenase/CP12/phosphoribulokinase complex. Journal of Experimental Botany **55**, 1245–1254.

Grunewald W, Friml J. 2010. The march of the PINs: developmental plasticity by dynamic polar targeting in plant cells. EMBO Journal **29**, 2700–2714.

Hawes C, Kiviniemi P, Kriechbaumer V. 2015 The endoplasmic reticulum: a dynamic and well-connected organelle. Journal of Integrative Plant Biology **57**, 50–62.

Hayashi K, Nakamura S, Fukunaga S, Nishimura T, Jenness MK, Murphy AS, Motose H, Nozaki H, Furutani M, Aoyama T (2014) Auxin transport sites are visualized in planta using fluorescent **auxin** analogs. Proceedings of the National Academy of Sciences 5 **111**, 11557–11562.

Hentrich M, Böttcher C, Düchting P, Cheng Y, Zhao Y, Berkowitz O, Masle J, Medina J, Pollmann S. 2013a. The jasmonic acid signaling pathway is linked to auxin homeostasis through the modulation of YUCCA8 and YUCCA9 gene expression. Plant Journal **74**, 626–637.

Hentrich M, Sánchez-Parra B, Pérez Alonso MM, Carrasco Loba V, Carrillo L, Vicente-Carbajosa J, Medina J, Pollmann S. 2013b. YUCCA8 and YUCCA9 overexpression reveals a link between auxin signaling and lignification through the induction of ethylene biosynthesis. Plant Signal Behaviour **8**, e26363.

Hornitschek P, Kohnen MV, Lorrain S, Rougemont J, Ljung K, López-Vidriero I, Franco-Zorrilla JM, Solano R, Trevisan M, Pradervand S *et al*. 2012. Phytochrome interacting factors 4 and 5 control seedling growth in changing light conditions by directly controlling auxin signaling. Plant Journal **71**, 699–711.

Jensen K, Osmani SA, Hamann T, Naur P, Moller BL. 2011. Homology modeling of the three membrane proteins of the dhurrin metabolon: catalytic sites, membrane surface association and protein-protein interactions. Phytochemistry **72**, 2113–2123.

Jørgensen K, Rasmussen AV, Morant M, Nielsen AH, Bjarnholt N, Zagrobelny M, Bak S, Møller BL. 2005. Metabolon formation and metabolic channeling in the biosynthesis of plant natural products. Current Opinion in Plant Biology **8**, 280–291.

Kang B, Wang H, Nam KH, Li J, Li J. 2010. Activation-tagged suppressors of a weak brassinosteroid receptor mutant. Molecular Plant **3**, 260–268.

Kasahara H. 2015. Current aspects of auxin biosynthesis in plants. Bioscience Biotechnology Biochemistry **80**, 34–42.

Kriechbaumer V, Park WJ, Gierl A, Glawischnig E. (2006) Auxin biosynthesis in maize. Plant Biology **8**, 334–339.

Kriechbaumer V, Park WJ, Piotrowski M, Meeley RB, Gierl A, Glawischnig E. 2007. Maize nitrilases have a dual role in auxin homeostasis and beta-cyanoalanine hydrolysis. Journal of Experimental Botany **58**, 4225–4233.

Kriechbaumer V, Wang P, Hawes C, Abell BM. 2012. Alternative splicing of the auxin biosynthesis gene YUCCA4 determines its subcellular compartmentation. Plant Journal **70**, 292–302.

Kriechbaumer V, Seo H, Park WJ, Hawes C. 2015a. Endoplasmic reticulum localization and activity of maize auxin biosynthetic enzymes. Plant Physiology **169**, 1933–1945.

Kriechbaumer V, Botchway SW, Slade SE, Knox K, Frigerio L, Oparka K, Hawes C. 2015b. Reticulomics: Protein-protein interaction studies with two plasmodesmata-localized reticulon family proteins identify binding partners enriched at plasmodesmata, endoplasmic reticulum, and the plasma membrane. Plant Physiology **169**,1933–1945.

Lallemand B, Erhardt M, Heitz T, Legrand M. (2013) Sporopollenin biosynthetic enzymes interact and constitute a metabolon localized to the endoplasmic reticulum of tapetum cells. Plant Physiology **162**, 616–625.

LeClere S, Schmelz EA, Chourey PS. 2010 Sugar levels regulate tryptophan-dependent auxin biosynthesis in developing maize kernels. Plant Physiology **153**, 306–318.

Lilley JL, Gee CW, Sairanen I, Ljung K, Nemhauser JL. 2012. An endogenous carbon-sensing pathway triggers increased auxin flux and hypocotyl elongation. Plant Physiology **160**, 2261–2270.

Llavata Peris CI, Rademacher EH, Weijers D. 2010. Green beginnings: pattern formation in the early plant embryo. In Plant Development: Current Topics in Developmental Biology **91**, Timmermans, M.C.P., ed. (Amsterdam: Elsevier), 1–27.

Mano Y, Nemoto K. 2012. The pathway of auxin biosynthesis in plants. Journal of Experimental Botany **63**, 2853–2872.

Møller BL. 2010. Dynamic metabolons. Science **330**, 1328–1329.

Mravec J, Skupa P, Bailly A, Hoyerova K, Krecek P, Bielach A, Petrasek J, Zhang J, Gaykova V, Stierhof YD, Dobrev PI, Schwarzerová K, Rolcík J, Seifertová D, Luschnig C, Benková E, Zazímalová E, Geisler M, Friml J. 2009. Subcellular homeostasis of phytohormone auxin is mediated by the ER localized PIN5 transporter. Nature **459**, 1136–1140.

Müller A, Weiler EW. 2000. IAA-synthase, an enzyme complex from Arabidopsis thaliana catalyzing the formation of indole-3-acetic acid from (S)-tryptophan. Journal of Biological Chemistry **381**, 679–686.

Nielsen KA, Tattersall DB, Jones PR, Moller BL. 2008. Metabolon formation in dhurrin biosynthesis. Phytochemistry **69**, 88–98.

Novák O, Hényková E, Sairanen I, Kowalczyk M, Pospíšil T, Ljung K. 2012. Tissue-specific profiling of the Arabidopsis thaliana auxin metabolome. Plant Journal **72**, 523–536.

Osterrieder A, Carvalho CM, Latijnhouwers M, Johansen JN, Stubbs C, Botchway S, Hawes C. 2009. Fluorescence lifetime imaging of interactions between Golgi tethering factors and small GTPases in plants. Traffic **10**, 1034–1046.

Park WJ, Kriechbaumer V, Müller A, Piotrowski M, Meeley RB, Gierl A, Glawischnig E. 2003. The nitrilase ZmNIT2 converts indole-3- acetonitrile to indole-3-acetic acid. Plant Physiology **133**, 794–802.

Perrot-Rechenmann C. 2010. Cellular responses to auxin: division versus expansion. Cold Spring Harb Perspect Biol **2**, a001446.

Pieck M, Yuan Y, Godfrey J, Fisher C, Zolj S, Vaughan D, Thomas N, Wu C, Ramos J, Lee N, Normanly J, Celenza JL. 2015 Auxin and Tryptophan Homeostasis Are Facilitated by the ISS1/VAS1 Aromatic Aminotransferase in Arabidopsis. Genetics **201**, 185–199.

Pollmann S, Düchting P, Weiler EW. 2009. Tryptophan-dependent indole-3-acetic acid biosynthesis by 'IAA-synthase' proceeds via indole-3- acetamide. Phytochemistry **70**, 523–531.

Ralston L, Yu O. 2006. Metabolons involving plant cytochrome P450s. Phytochemistry Reviews **5**, 459–472.

Runions J, Brach T, Kuhner S, Hawes C. 2006. Photoactivation of GFP reveals protein dynamics within the endoplasmic reticulum membrane. Journal of Experimental Botany **50**, 43–50.

Sairanen I, Novák O, Pencík A, Ikeda Y, Jones B, Sandberg G, Ljung K. (2012). Soluble carbohydrates regulate auxin biosynthesis via PIF proteins in Arabidopsis. Plant Cell **24**, 4907–4916.

Sawchuk MG, Edgar A, Scarpella E. 2013. Patterning of leaf vein networks by convergent auxin transport pathways. PLoS Genetics **9**, e1003294.

Sage RF. 2002. Variation in the k(cat) of Rubisco in C(3) and C(4) plants and some implications for photosynthetic performance at high and low temperature. Journal of Experimental Botany **53**, 609–620.

Scarpella E, Marcos D, Friml J, Berleth T. 2006. Control of leaf vascular patterning by polar auxin transport. Genes & Development **20**, 1015–1027.

Srere PA. 1985. The metabolon. Trends in Biochemical Sciences **10**, 109–110.

Stepanova AN, Robertson-Hoyt J, Yun J, Benavente LM, Xie DY, Dolezal K, Schlereth A, Jürgens G, Alonso JM. 2008. TAA1-mediated auxin biosynthesis is essential for hormone crosstalk and plant development. Cell **133**, 177-191.

Sun J, Qi L, Li Y, Chu J, Li C. 2012 PIF4-mediated activation of YUCCA8 expression integrates temperature into the auxin pathway in regulating arabidopsis hypocotyl growth. PLoS Genetics **8**,e1002594.

Sundberg E, Østergaard L. 2009. Distinct and dynamic auxin activities during reproductive development. Cold Spring Harbour Perspectives in Biology **1**, a0012628.

Tao Y, Ferrer JL, Ljung K, Pojer F, Hong F, Long JA, Li L, Moreno JE, Bowman ME, Ivans LJ, Cheng Y, Lim J, Zhao Y, Ballaré CL, Sandberg G, Noel JP, Chory J. 2008. Rapid synthesis of auxin via a new tryptophan-dependent pathway is required for shade avoidance in plants. Cell **133**, 164-76.

Tivendale ND, Ross JJ, Cohen JD. 2014. The shifting paradigm of auxin biosynthesis. Trends in Plant Science **19**, 44–51.

Torii KU, Mitsukawa N, Oosumi T, Matsuura Y, Yokoyama R, Whittier RF, Komeda Y. 1996. The Arabidopsis ERECTA gene encodes a putative receptor protein kinase with extracellular leucine-rich repeats. Plant Cell **8**, 735–46.

Tzin V, Galili G. 2010. The biosynthetic pathways for shikimate and aromatic amino acids in Arabidopsis thaliana. The Arabidopsis Book **8**, e0132.

Wang B, Chu J, Yu T. 2015. Tryptophan-independent auxin biosynthesis contributes to early embryogenesis in *Arabidopsis*. Proc. Nat. Acad. Sci. USA **112**, 4821–4826.

Woodward AW, Bartel B. 2005. Auxin: regulation, action, and interaction. Annals of Botany **95**, 707–735.

Woodward C, Bemis SM, Hill EJ, Sawa S, Koshiba T, Torii KU. 2005b. Interaction of auxin and ERECTA in elaborating Arabidopsis inflorescence architecture revealed by the activation tagging of a new member of the YUCCA family putative flavin monooxygenases. Plant Physiology **139**, 192–203.

Xie Y, Straub D, Eguen T, Brandt R, Stahl M, Martínez-García JF, Wenkel S. 2015. Meta-Analysis of Arabidopsis KANADI1 Direct Target Genes Identifies a Basic Growth-Promoting Module Acting Upstream of Hormonal Signaling Pathways. Plant Physiology **169**, 1240–1253.

Yamada M, Greenham K, Prigge MJ, Jensen PJ, Estelle M. 2009. The TRANSPORT INHIBITOR RESPONSE2 gene is required for auxin synthesis and diverse aspects of plant development. Plant Physiology **151**, 168–179.

Zajchowski LD, Robbins SM. 2002. Lipid rafts and little caves. European Journal of Biochemistry **269**, 737–752.

Zhao Y, Christensen SK, Fankhauser C, Cashman JR, Cohen JD, Weigel D, Chory J. 2001. A role for flavin monooxygenase-like enzymes in auxin biosynthesis. Science **291**, 306–309.

Zhao Y. 2010. Auxin biosynthesis and its role in plant development. Annual Review of Plant Biology **61**, 49–64.

Zhou ZY, Zhang CG, Wu L, Zhang CG, Chai J, Wang M, Jha A, Jia PF, Cui SJ, Yang M *et al*. 2011. Functional characterization of the CKRC1/TAA1 gene and dissection of hormonal actions in the Arabidopsis root. Plant Journal **66**, 516–527.

Tables

Table 1. In silico prediction of targeting sequences identified by WoLFPSORT or TargetP 1.1. TMDs were predicted using the computational algorithms TMHMM, signal peptides using SignalP4.1 (http://www.expasy.org/tools/).

Enzyme	TMD predicted by TMHMM (position; N-terminus)	Targeting Sequences by WoLFPSORT (residues) [TargetP 1.1]	Localisation (evidence)	Gene ID, Length [aa] & Expression
YUC1	0	NLS	Nucleus (sequence analysis)	AT4G32540.1 414 Ubiquitously expressed
YUC2	0	None (evidence of NLS)	Cytosol or possibly nucleus (sequence analysis)	AT4G13260.1 415 Ubiquitously expressed
YUC3	1 (31-53; in)	None (evidence of PTS1)	Cytosol or possibly peroxisome (sequence analysis)	AT1G04610.1 437 Ubiquitously expressed
YUC4.1	0	None	Cytosol (Kriechbaumer *et al*. 2012)	AT5G11320.1 411 Ubiquitously expressed
YUC4.2	1 (334-356; out)	None	ER membrane - cytosolic N-terminus (Kriechbaumer *et al*. 2012)	AT5G11320.2 357 Flower
YUC5	1 (248-270; out)	Signal-anchor (251-267)	ER membrane - cytosolic N-terminus (sequence analysis)	AT5G43890.1 424 Cotyledon, guard cell, root, vascular leaf
YUC6.1	aa 21-50 below threshold 0	None	Non-cytosolic (Kim *et al*. 2007)	AT5G25620.1 417 Guard cell, flower
YUC6.2	aa 13-42 below threshold	None	Non-cytosolic (Kim *et al*. 2007)	AT5G25620.2 426 Guard cell, flower
YUC7	0	Nucleus	Nucleus or chloroplast (sequence analysis)	AT2G33230.1 431 Drought-induced
YUC8	0 - 251-267 below threshold	ER (Signal-anchor 251-267)	ER membrane - cytosolic N-terminus (sequence analysis)	AT4G28720.1 426 Ubiquitously expressed
YUC9	0 - 250-266 below threshold	ER (Signal-anchor 250-266)	ER membrane - cytosolic N-terminus (sequence analysis)	AT1G04180.1 421 Root
YUC10	0	None cytosol	Cytosol (sequence analysis)	AT1G48910.1 383 Pollen
YUC11	0 - 7-23 below threshold	Possible signal-anchor (7-23) [ER]	ER membrane - cytosolic C-terminus (sequence analysis)	AT1G21430.1 391 Leaf
TAA1	0	None	Cytosol (sequence analysis)	AT1G70560.1 391 Ubiquitously expressed
TAR1	0	None	Cytosol	AT1G23320.1

			(sequence analysis)	388 Ubiquitously expressed
TAR2	1 (7-26; in)	ER (Signal-anchor 13-29) [ER]	ER membrane - cytosolic C-terminus (sequence analysis)	AT4G24670.1 440 Ubiquitously expressed

Table 2: Fluorescence lifetimes FRET-FLIM analysis.

Donor and acceptor protein constructs are indicated together with the average fluorescence lifetime (in ns) for the donor fluorophore and the standard error for each combination. Δ indicates the change in life time in comparison to the donor control without acceptor present.

Donor	Acceptor	GFP-fluorescence lifetime [ns]	Δ [ns]
TAR2-GFP	(-)	3.1 ± 0.03	0.0
	YUC1-mCherry	3.0 ± 0.04	0.0
	YUC2-mCherry	3.0 ± 0.05	0.0
	YUC3-mCherry	3.0 ± 0.06	0.0
	YUC5-mCherry	2.8 ± 0.03	0.3
	YUC6-mCherry	3.0 ± 0.05	0.0
	YUC7-mCherry	3.0 ± 0.05	0.0
	YUC8-mCherry	2.8 ± 0.02	0.2
	YUC9-mCherry	3.0 ± 0.05	0.0
	YUC11-mCherry	3.0 ± 0.05	0.0
GFP-YUC5	(-)	2.5 ± 0.02	0.0
	YUC5-mCherry	2.3 ± 0.03	0.2
	YUC6-mCherry	2.5 ± 0.01	0.0
	YUC7-mCherry	2.3 ± 0.01	0.2
	YUC8-mCherry	2.5 ± 0.01	0.0
	YUC9-mCherry	2.3 ± 0.02	0.2
	YUC11-mCherry	2.3 ± 0.01	0.2
	TAA-mCherry	2.5 ± 0.02	0.0
YUC8-GFP	(-)	2.5 ± 0.02	0.0
	YUC5-mCherry	2.6 ± 0.03	0.0
	YUC6-mCherry	2.6 ± 0.03	0.0
	YUC7-mCherry	2.4 ± 0.04	0.2
	YUC8-mCherry	2.4 ± 0.01	0.2
	YUC9-mCherry	2.5 ± 0.03	0.0
	YUC11-mCherry	2.5 ± 0.00	0.0
	TAA-mCherry	2.5 ± 0.05	0.0

Figure legends

Figure 1: Transient expression and localization of auxin biosynthetic proteins in tobacco leaf cells.

Co-expression with the ER luminal marker GFP–HDEL (green) is shown for the TAA/TAR proteins TAR2 and TAA1 (A). YUC5, YUC7, YUC8, and YUC9 fused to mCherry (pink) colocalise with the ER marker GFP HDEL (B). YUC1, YUC2, YUC3, YUC6, and YUC11 show a cytosolic distribution and do not colocalise with GFP-HDEL (C). Red size bar = 5µm.

Figure 2: Leaf curling bioassay to determine the functionality of tagged enzymes. Expression of a combination of TAA/TAR and YUC results in leaf bending; two TAA/TAR proteins or two YUC proteins do not have this effect. Examples shown here are YUC5/TAA1 (A) and YUC2/TAR2 (B) for leaf bending (right hand side of leaves) and YUC2/YUC5 (A) and TAA1/TAR2 (B) combined (left hand side of leaves). An IAA solution was infiltrated as a control (C, right hand side of leaf). Front and side views for each leaf are shown.

Figure 3: Immunoblot analysis of microsomal fractions.

Immunoblot analysis of Hsp70 proteins in the Arabidopsis seedling cytosolic (C) and microsomal (M) fraction and immunoblot analysis of plasma membrane H^+ATPase proteins and mitochondrial alternative oxidases (AOX1/2) in the Arabidopsis total protein extract (T) and microsomal (M) fraction. Western blots of 100 µg of protein from each fraction were probed with diluted (1:1000) antibodies. Anti-Hsp70 recognize the cytosolic Hsp70 protein, anti-H^+ATPase antibodies detect the plasma membrane localised H^+ATPase protein and anti-AOX1/2 antibodies bind the mitochondrial AOX1/2 protein.

Figure 4: Enzymatic conversion of tryptophan (grey bars) and IPyA (white bars) to IAA by microsomal (Micro) fractions, cytosolic (Cyt) fractions, or total plant extract (Total) of Arabidopsis seedlings 5 d after germination. Standard errors and percentages normalized to total plant extract are indicated. *n*=2 (two biological samples with three replicates each).

Figure 5: FRET-FLIM analysis of TAR2 without an interaction partner (A–E) or with YUC5 (F–J) or YUC9 (K-O), respectively.

A, F and K display the raw FRET-FLIM data. The pseudo-coloured lifetime maps in B, G and L show the lifetime values for each point within the region of interest, whist the distribution of lifetimes across the image is shown in C, H and M. Blue shades representing longer GFP fluorescence lifetimes than green ones. D, I and N display representative decay curves of a single point with an optimal single exponential fit, where χ^2 values from 0.9 to 1.2 were considered an excellent fit to the data points (binning factor of 2 was applied). The confocal images for the analysis in E, J and O show the GFP-construct in green and the m-Cherry construct in red.

This example of FRET-FLIM analysis shows TAR2-GFP alone as a negative control, YUC5 for protein-protein interaction and YUC9 for no interaction with TAR2. The fluorescence lifetime values for TAR2-GFP+YUC5-mCherry are 2.92 ± 0.03 ns and therefore statistically lower than the lifetime values for the TAR2-GFP fusion alone (3.04 ± 0.03 ns). In contrast the lifetime value for the donor-acceptor combination TAR2-GFP/YUC9-mCherry is with 3.05 ± 0.06 ns not statistically different from the negative control, TAR2-GFP alone, hence indicating that TAR2 and YUC9 do not interact.

Figure 6: Fluorescence lifetimes in FRET-FLIM interactions with TAA/TAR and YUC proteins.

The bar graphs represent average fluorescence lifetimes (ns) and the corresponding SE values for the GFP donors TAR2 (A), YUC5 (B), and YUC8 (C). The data show the candidate interaction proteins (blue bars) compared with TAR2-GFP, GFP-YUC5 or YUC8-GFP without interaction partners (grey bars). Lifetimes significantly lower than those of TAR2-GFP, GFP-YUC5 or YUC8-GFP alone (lower than blue line) indicate protein-protein interactions.

Supplementary data

Supplementary Figure S1: Colocalisation of auxin biosynthetic proteins with the ER-marker GFP-HDEL. Pearson-Spearman coefficients and scatterplots using the ImageJ plug-in PSC (French *et al*., 2008) are listed and representative scatter plots shown.

Supplementary Figure S2: Stable expression of TAR2-mCherry in *Arabidopsis thaliana*. TAR2-mCherry labels the ER network in Arabidopsis.

Supplementary Figure S3: Representative FRE-FLIM data for interactions tested with TAR2-GFP, GFP-YUC5, or YUC8-GFP, respectively, as donor proteins. Corresponding confocal images with the GFP constructs in green and tested interacting proteins in red are shown on the right hand side.

Supplementary Figure S4: Transient expression and colocalisation of in tobacco leaf cells.
The auxin biosynthetic proteins YUC5-mCherry and YUC8-mCherry are co-expression with TAR2-GFP. Red size bar = 5µm.

Figure 1A

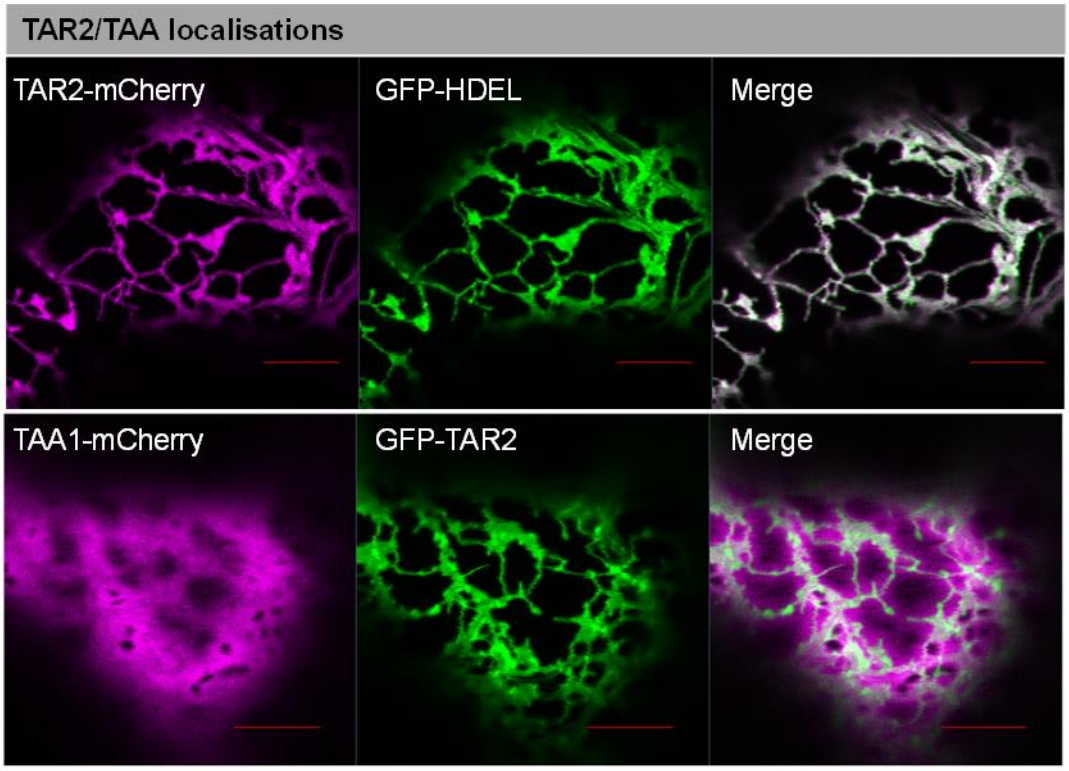
TAR2/TAA localisations
TAR2-mCherry
GFP-HDEL
Merge
TAA1-mCherry
GFP-TAR2
Merge

Figure 1B

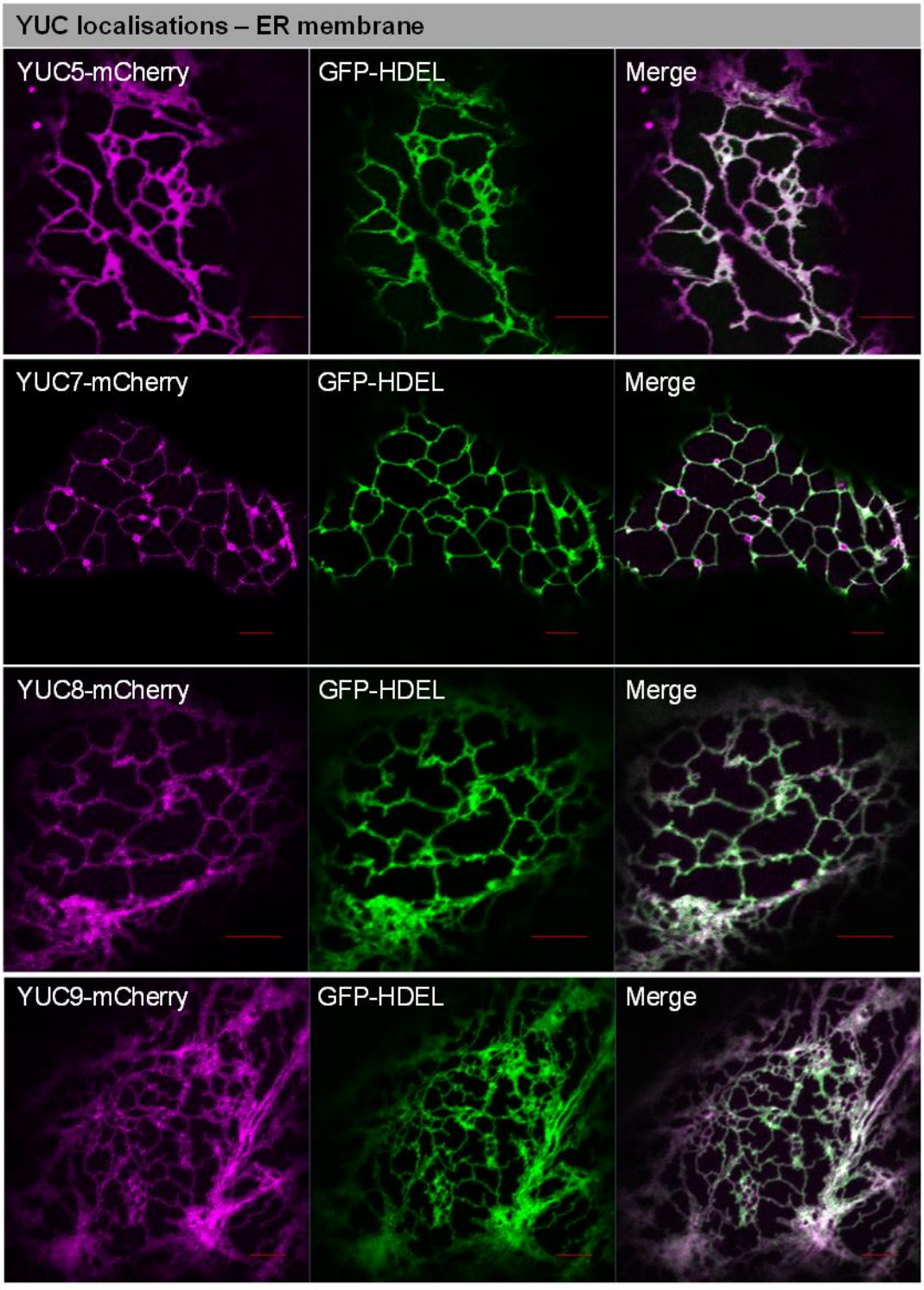
YUC localisations – ER membrane
YUC5-mCherry
GFP-HDEL
Merge
YUC7-mCherry
GFP-HDEL
Merge
YUC8-mCherry
GFP-HDEL
Merge
YUC9-mCherry
GFP-HDEL
Merge

Figure 1C

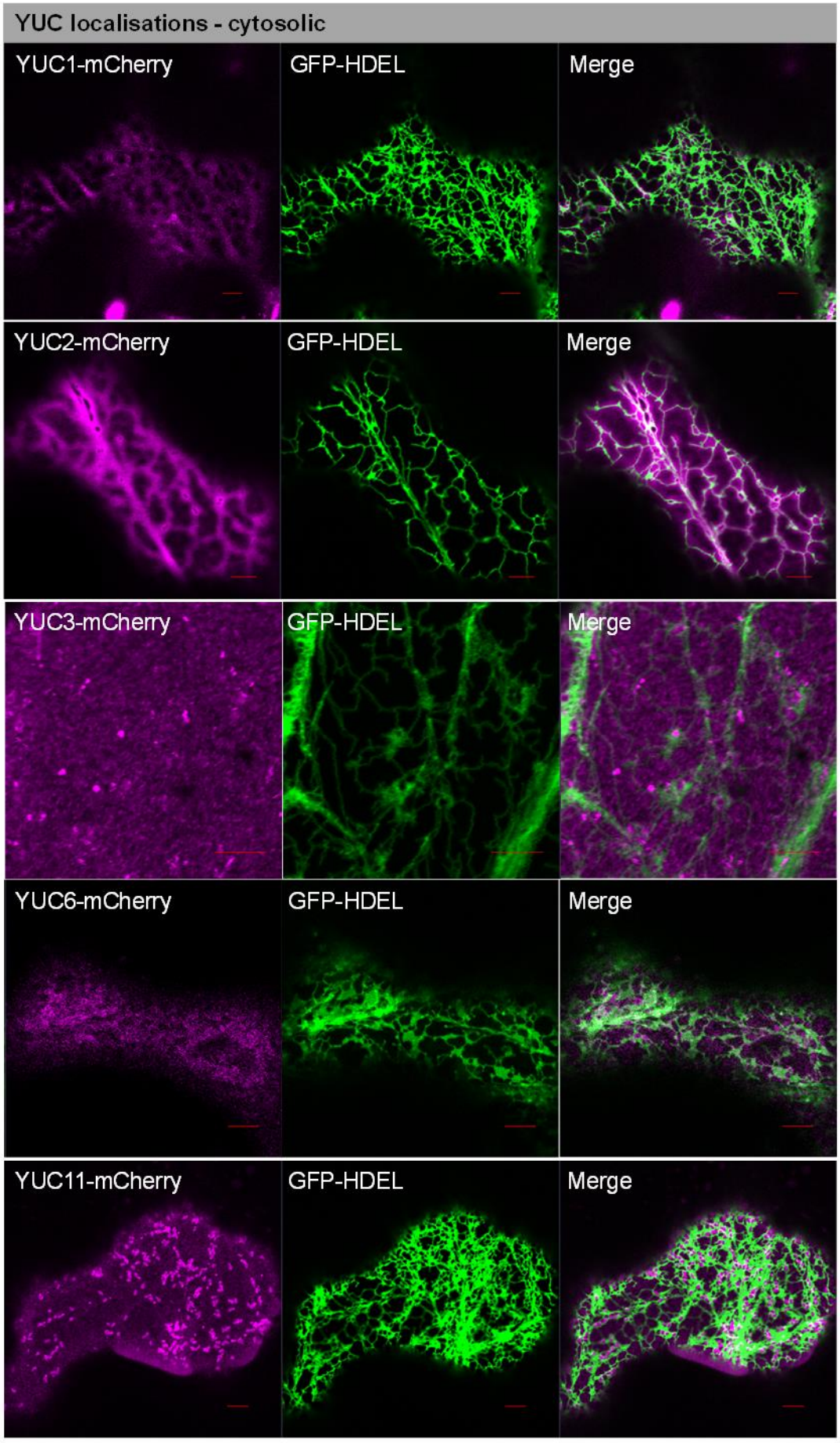
YUC localisations - cytosolic
YUC1-mCherry
GFP-HDEL
Merge
YUC2-mCherry
GFP-HDEL
Merge
YUC3-mCherry
GFP-HDEL
Merge
YUC6-mCherry
GFP-HDEL
Merge
YUC11-mCherry
GFP-HDEL
Merge

Figure 2

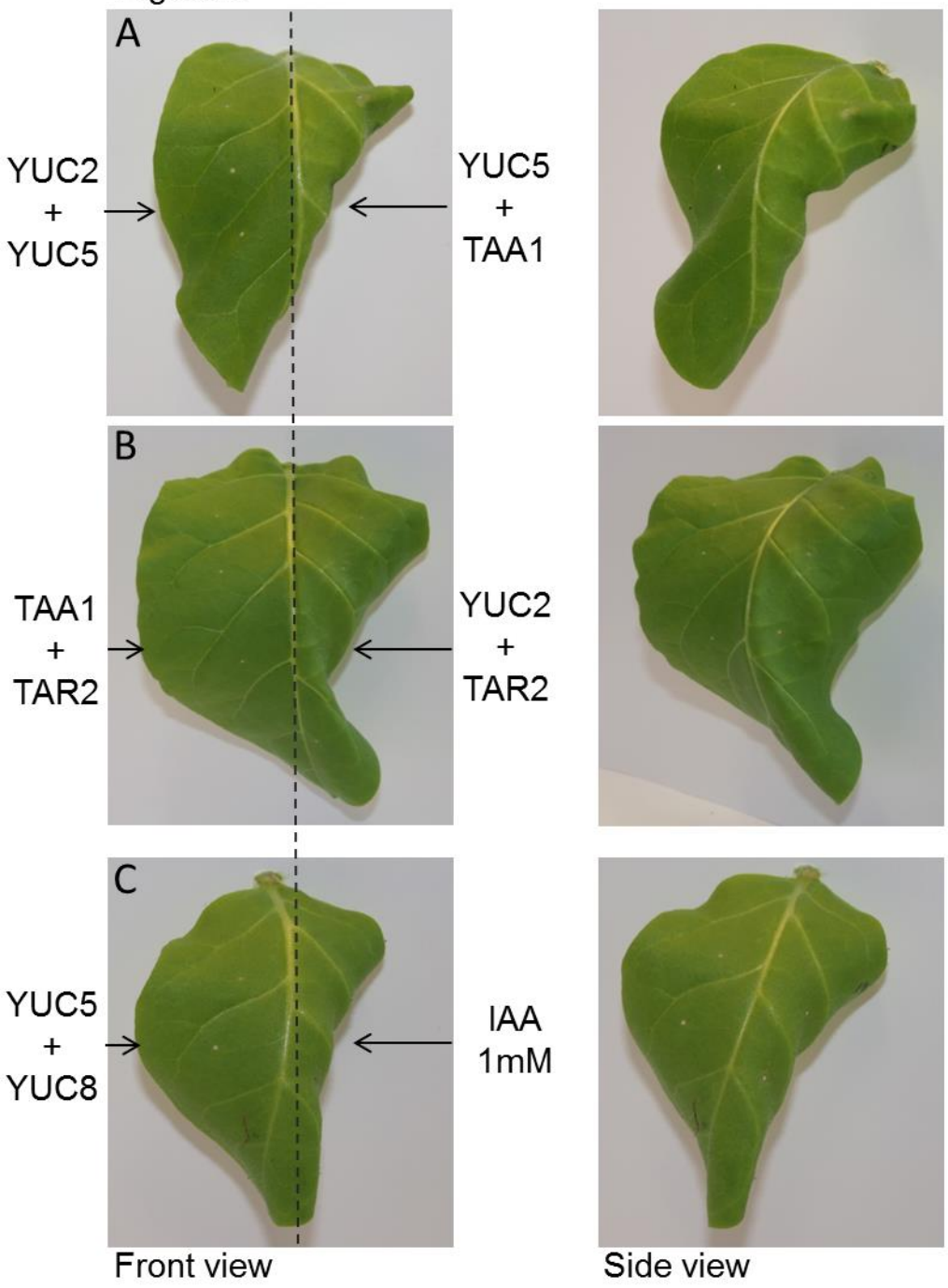
A
YUC2
+
YUC5
YUC5
+
TAA1
B
TAA1
+
TAR2
YUC2
+
TAR2
C
YUC5
+
YUC8
IAA
1mM
Front view
Side view

Figure 3

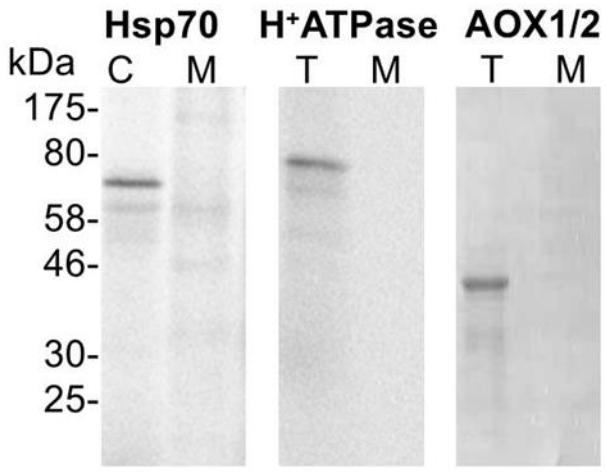

Figure 4

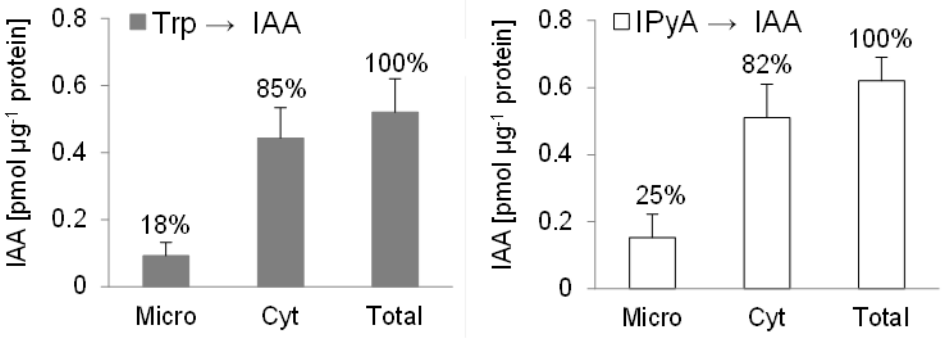
Trp → IAA
IAA [pmol µg-1 protein]
0.8
0.6
0.4
0.2
0
18%
85%
100%
Micro
Cyt
Total
IPyA → IAA
IAA [pmol µg-1 protein]
0.8
0.6
0.4
0.2
0
25%
82%
100%
Micro
Cyt
Total

Figure 5

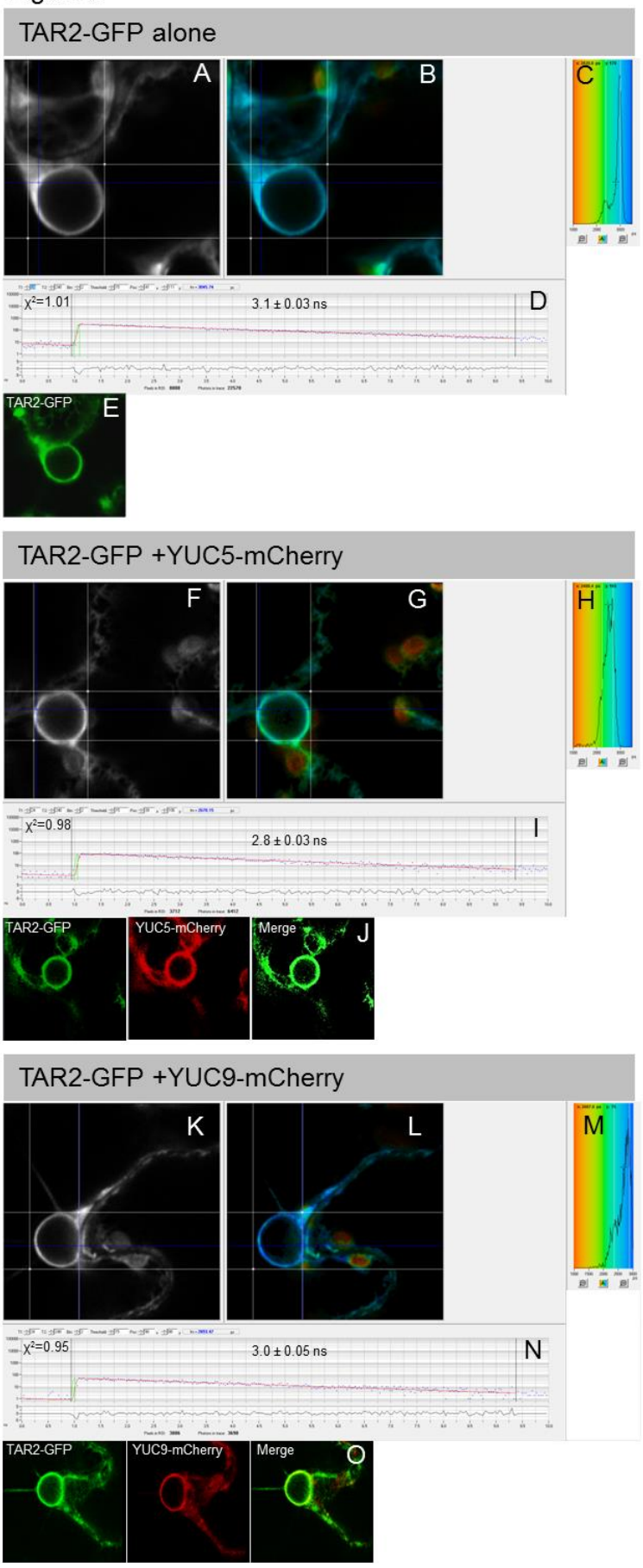
TAR2-GFP alone
A
B
C
χ²=1.01
3.1 ± 0.03 ns
D
TAR2-GFP
E
TAR2-GFP +YUC5-mCherry
F
G
H
χ²=0.98
2.8 ± 0.03 ns
I
TAR2-GFP
YUC5-mCherry
Merge
J
TAR2-GFP +YUC9-mCherry
K
L
M
χ²=0.95
3.0 ± 0.05 ns
N
TAR2-GFP
YUC9-mCherry
Merge
O

Figure 6A

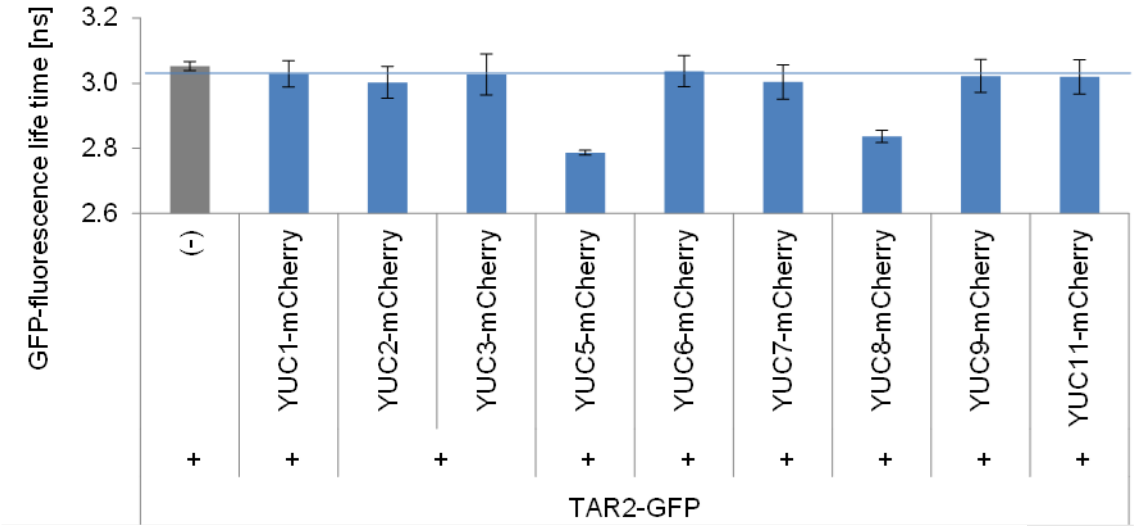

Figure 6B

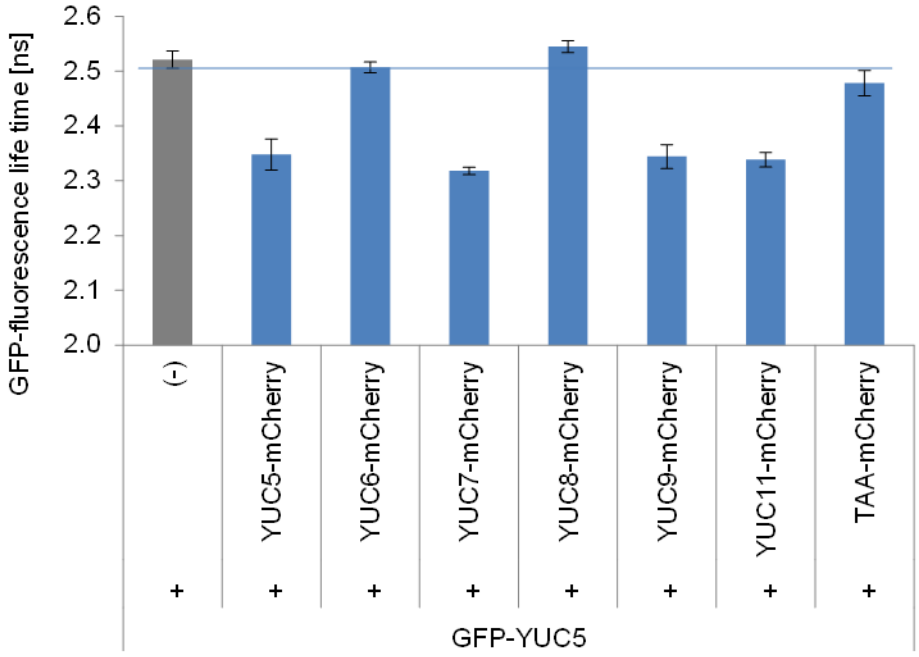

Figure 6C

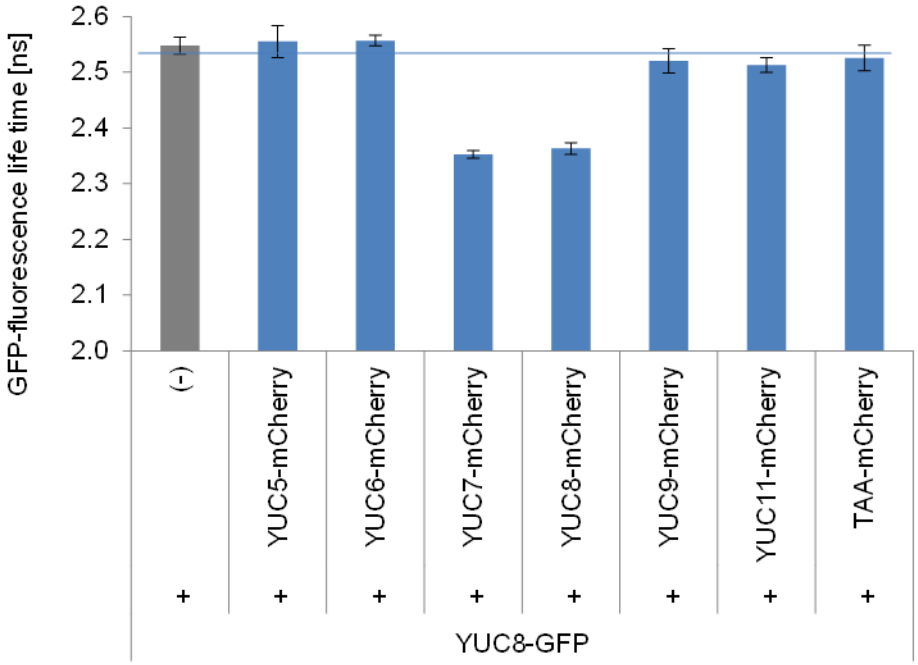
GFP-fluorescence life time [ns]
2.6
2.5
2.4
2.3
2.2
2.1
2.0
(-)
YUC5-mCherry
YUC6-mCherry
YUC7-mCherry
YUC8-mCherry
YUC9-mCherry
YUC11-mCherry
TAA-mCherry
+
+
+
+
+
+
+
+
YUC8-GFP

Supplementary Figure S1

Protein combination	Pearson's r coefficient	Location: ER/cytosol
TAR2-mCherry + GFP-HDEL	0.36	ER
TAA-mCherry + GFP-HDEL	0.09	cytosol
YUC5-mCherry + GFP-HDEL	0.35	ER
YUC7-mCherry + GFP-HDEL	0.32	ER
YUC8-mCherry + GFP-HDEL	0.31	ER
YUC9-mCherry + GFP-HDEL	0.4	ER
YUC1-mCherry + GFP-HDEL	0.08	cytosol
YUC2-mCherry + GFP-HDEL	0.06	cytosol
YUC3-mCherry + GFP-HDEL	0.08	cytosol
YUC6-mCherry + GFP-HDEL	0.07	cytosol
YUC11-mCherry + GFP-HDEL	0.02	cytosol

Representative scatter plots:

TAR2+HDEL YUC5+HDEL YUC9+HDEL YUC1+HDEL

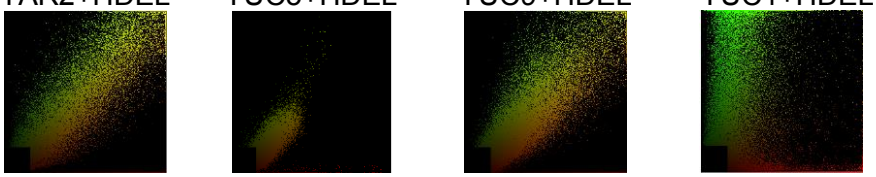

Supplementary Figure S2

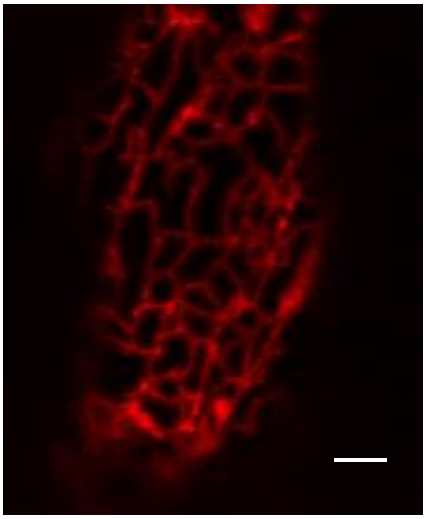

Supplementary Figure S3

clover-TAR2 +

(-)

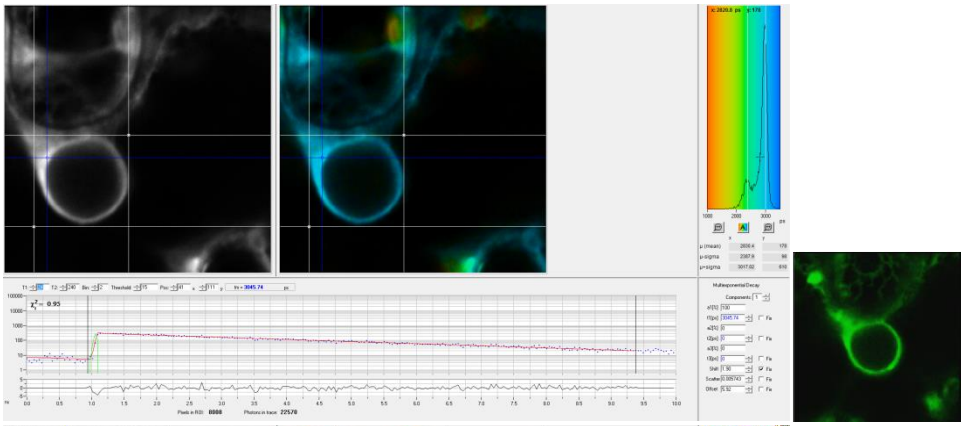

YUC1

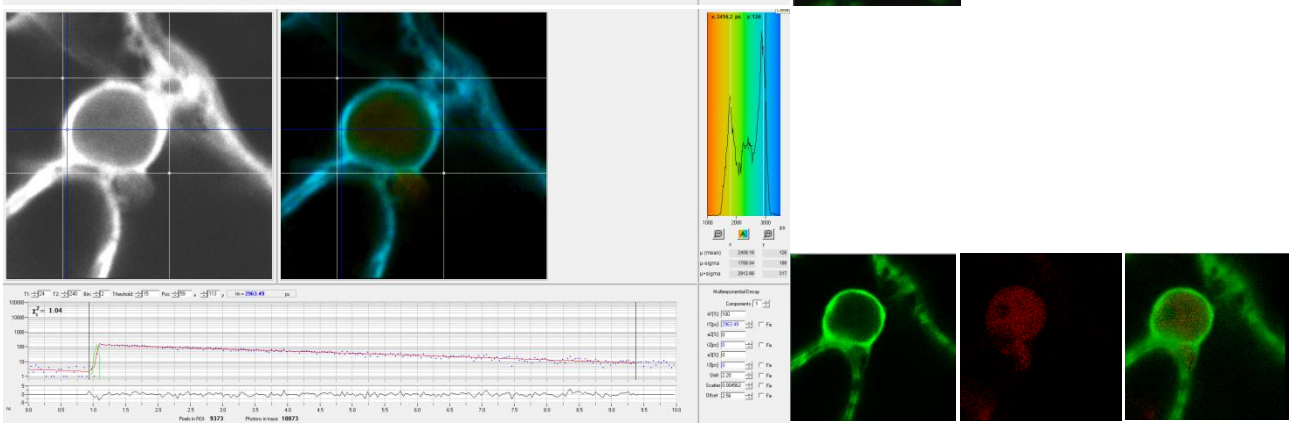

YUC2

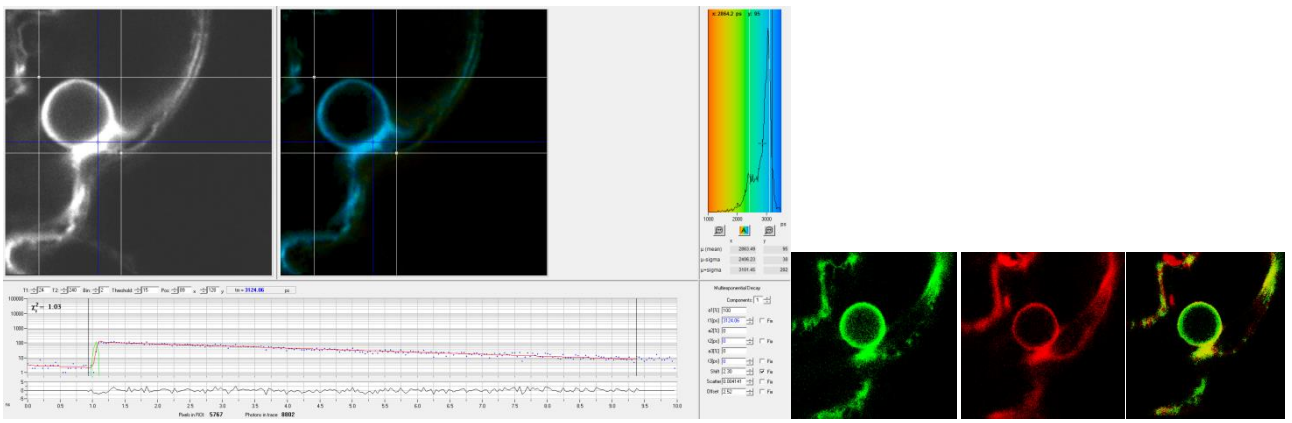

YUC3

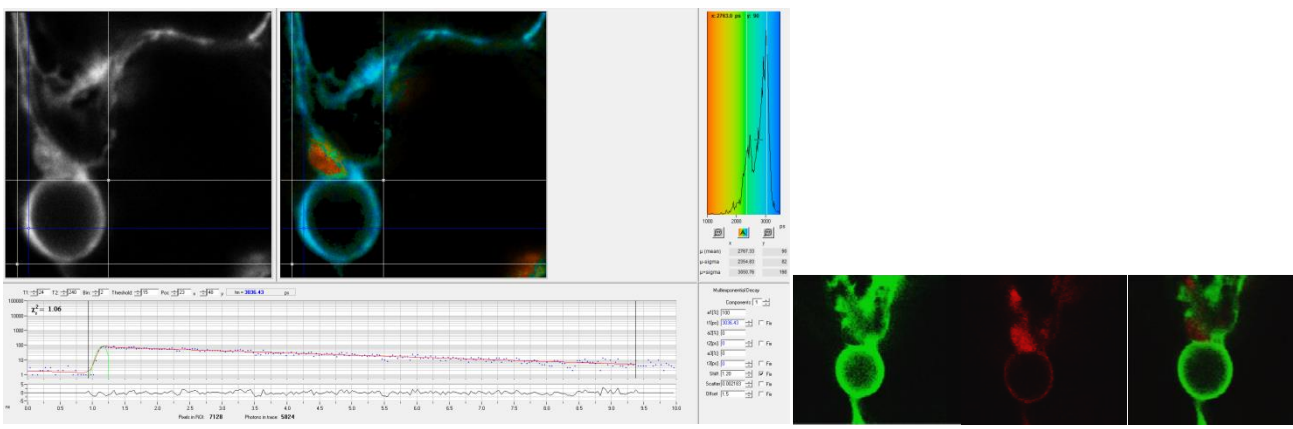

clover-TAR2 +

YUC6

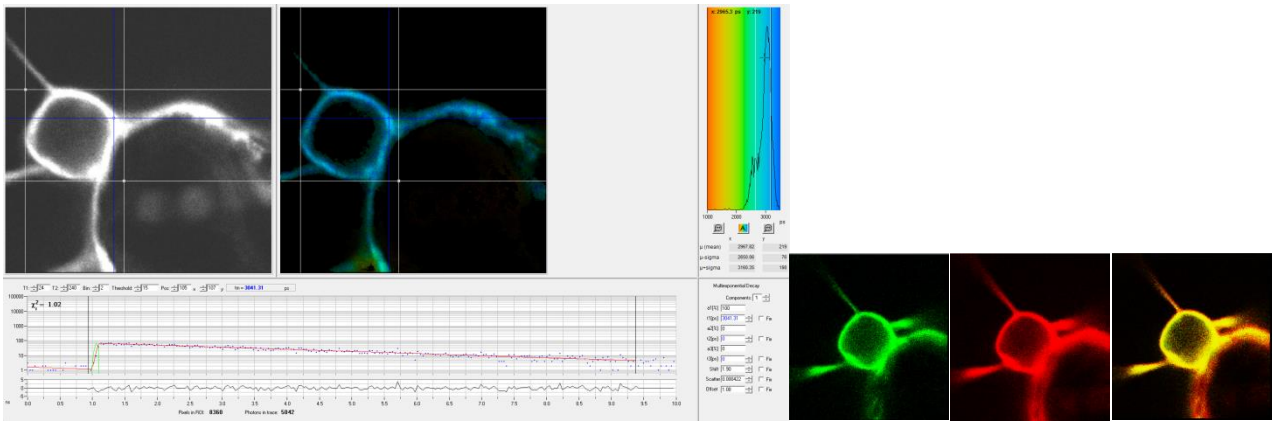

YUC7

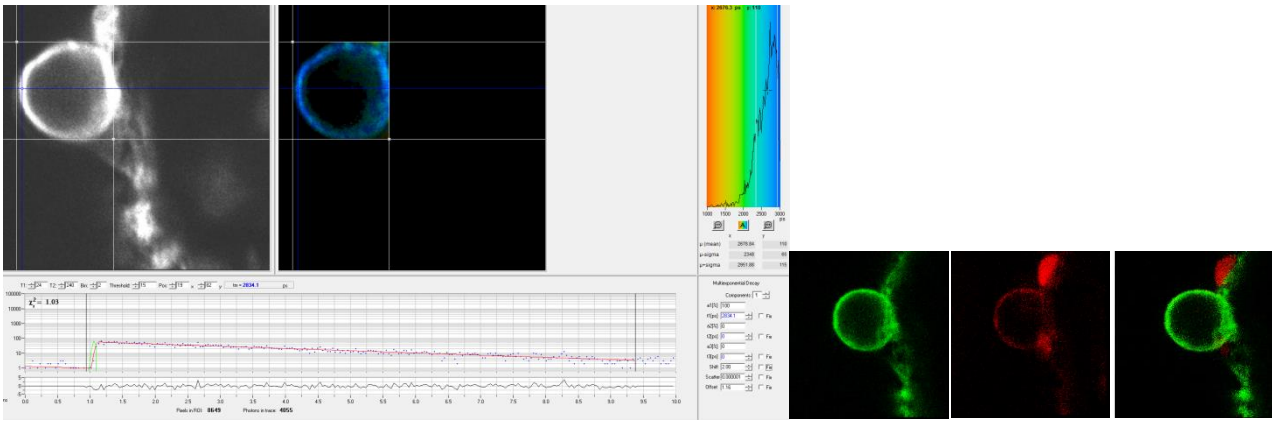

YUC8

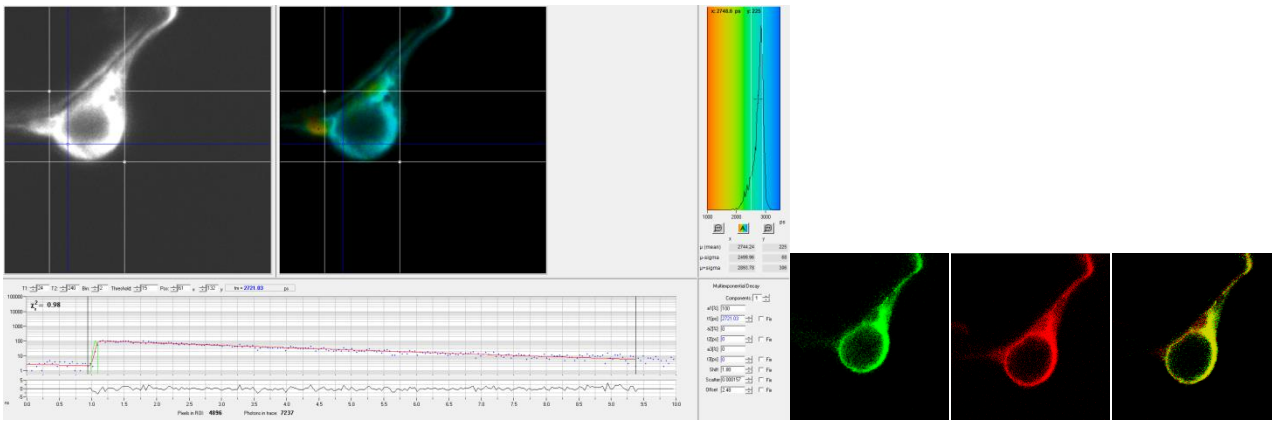

YUC11

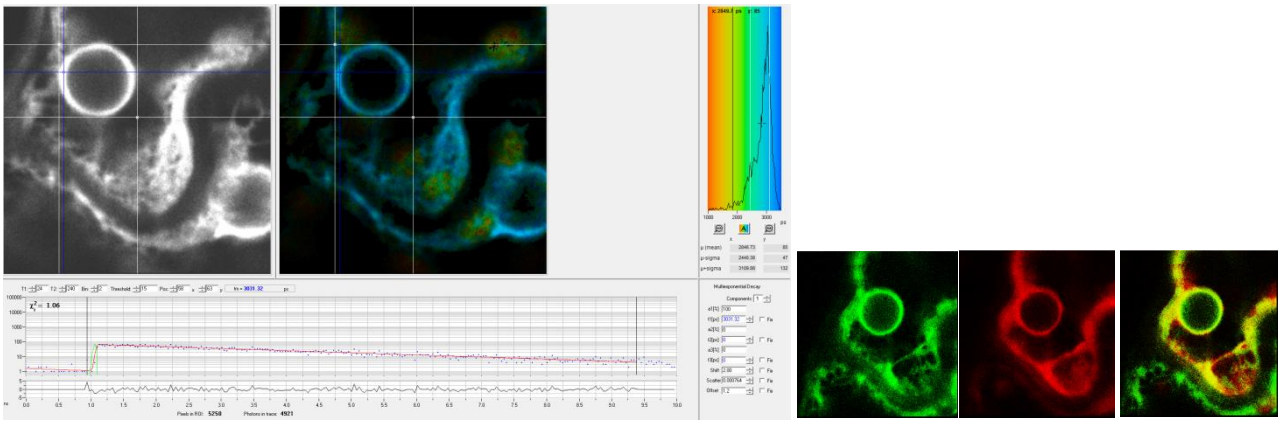

GFP-YUC5 +

(-)

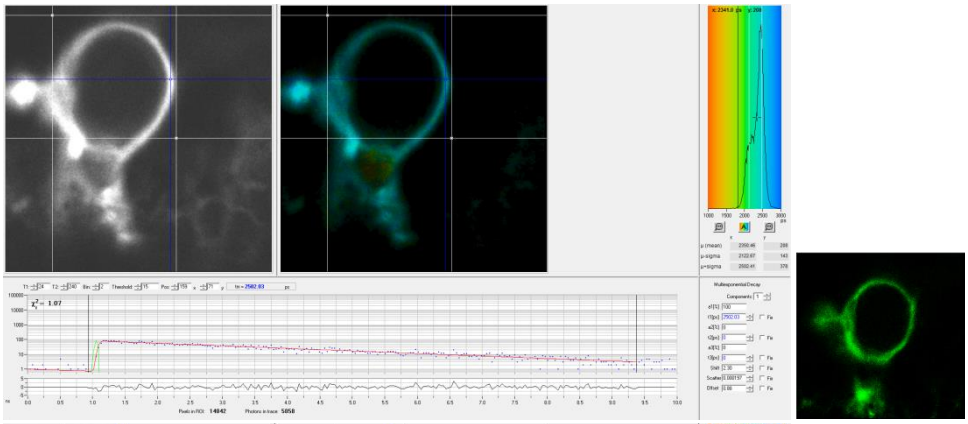

YUC5

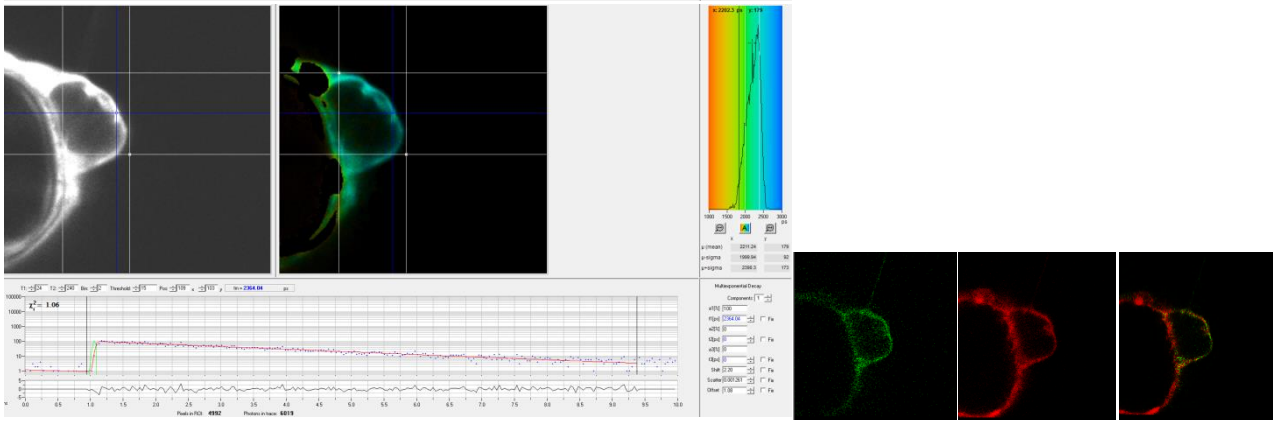

YUC6

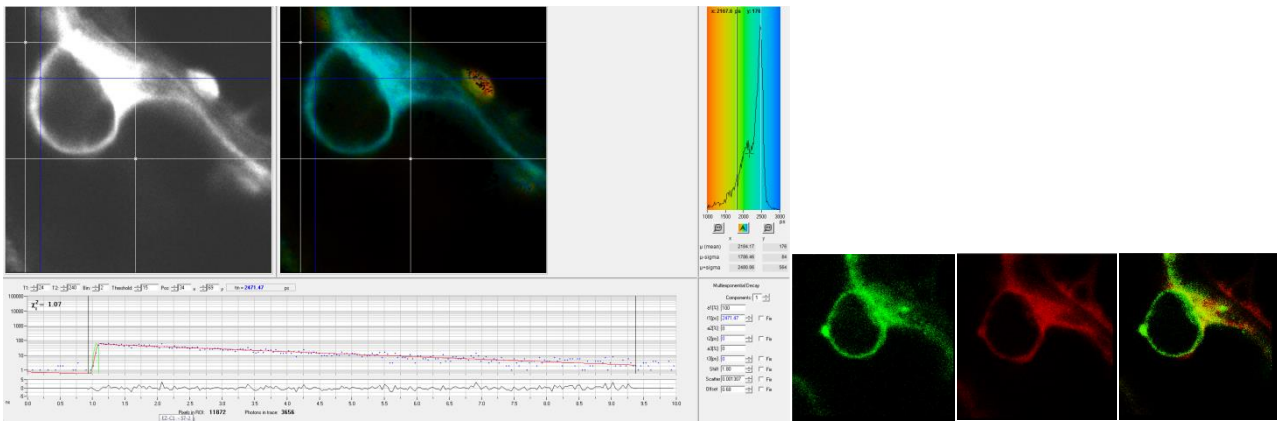

YUC7

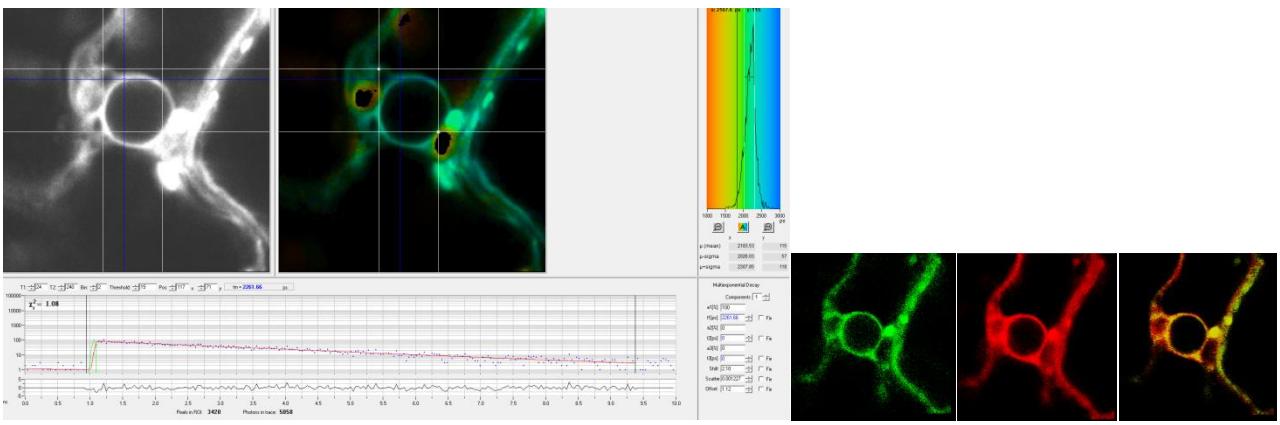

GFP-YUC5 +

YUC8

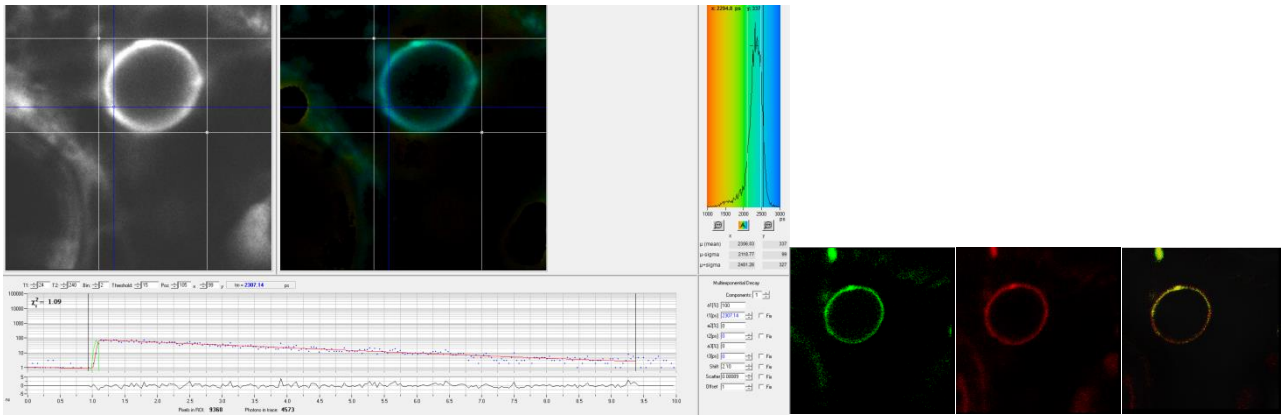

YUC9

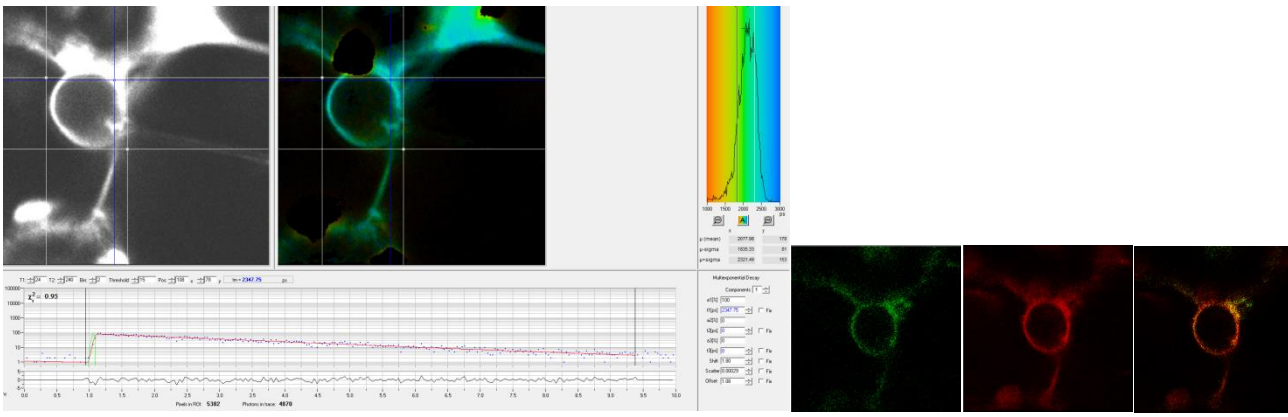

YUC11

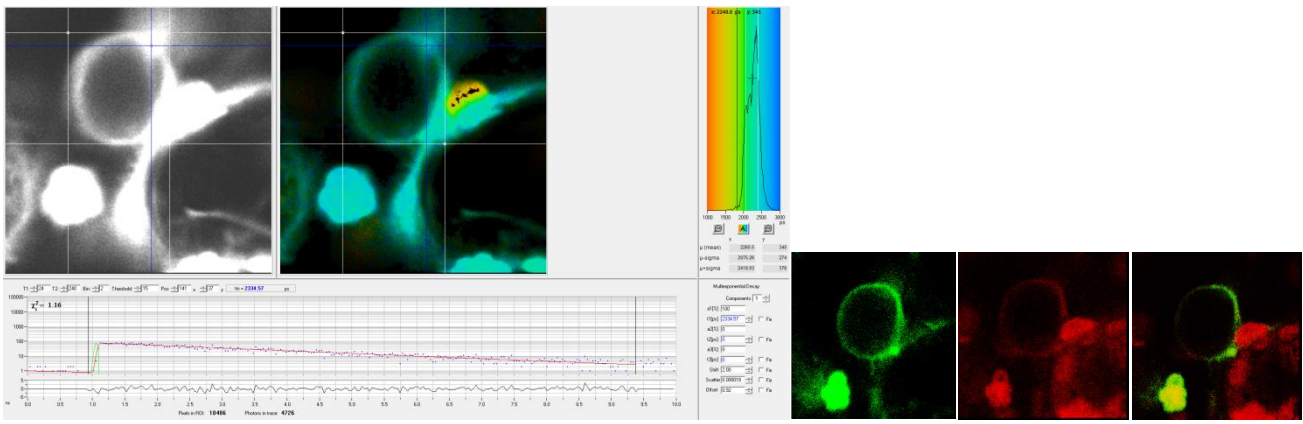

TAA1

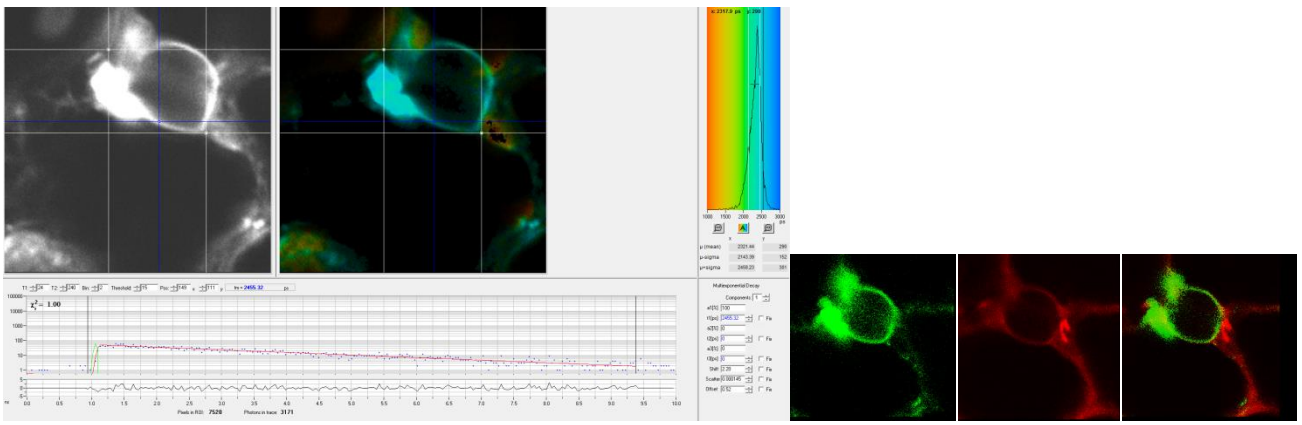

YUC8-GFP +

(-)

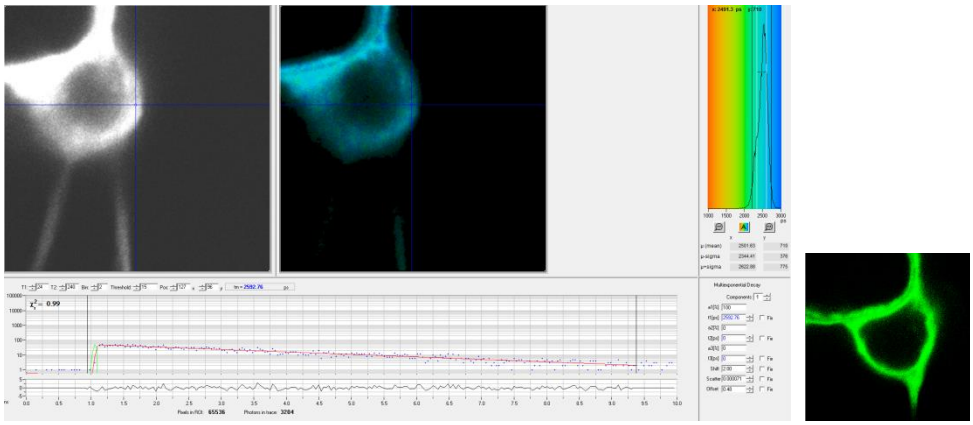

YUC5

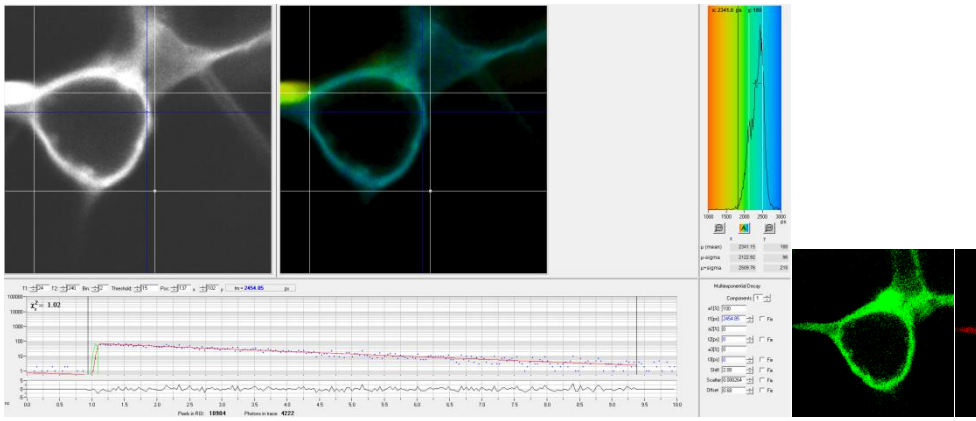

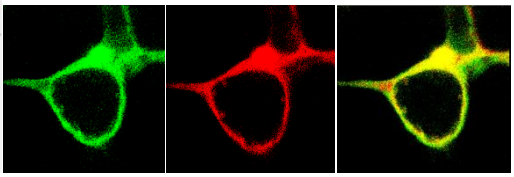

YUC6

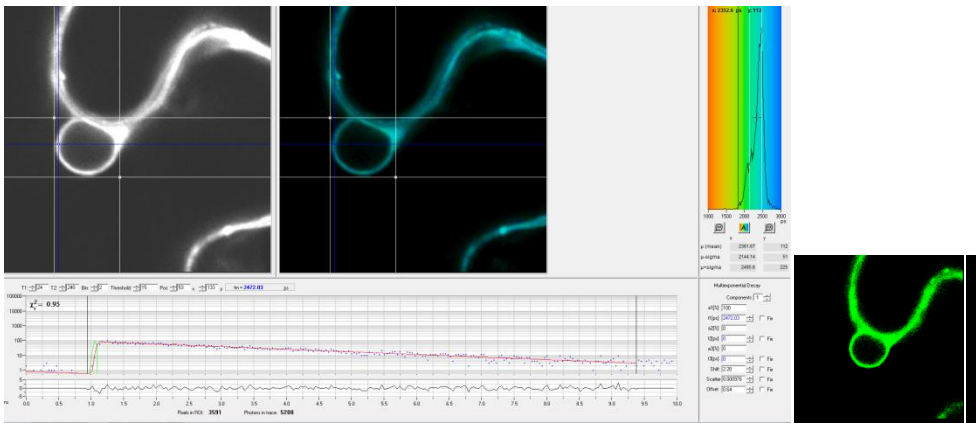

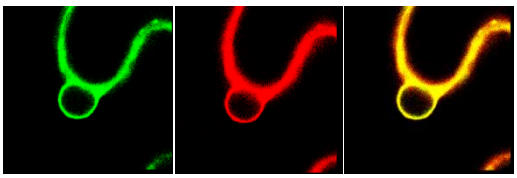

YUC7

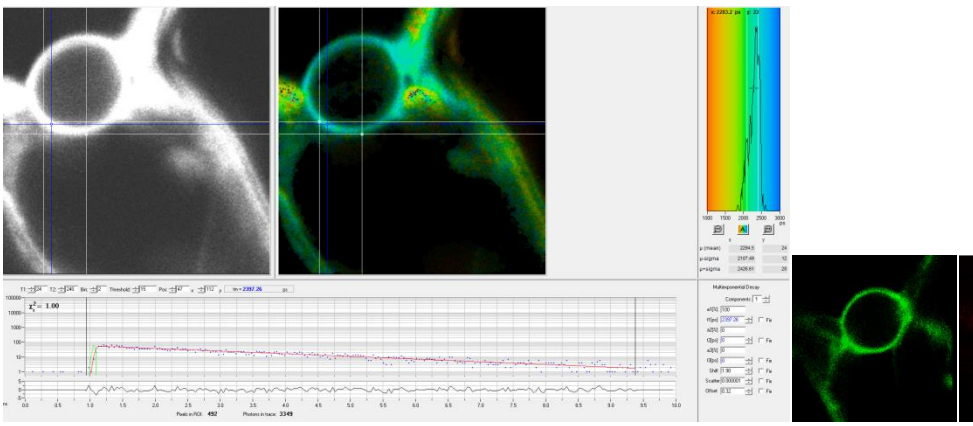

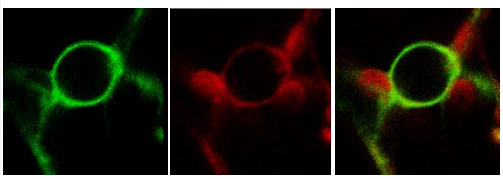

YUC8-GFP +

YUC8

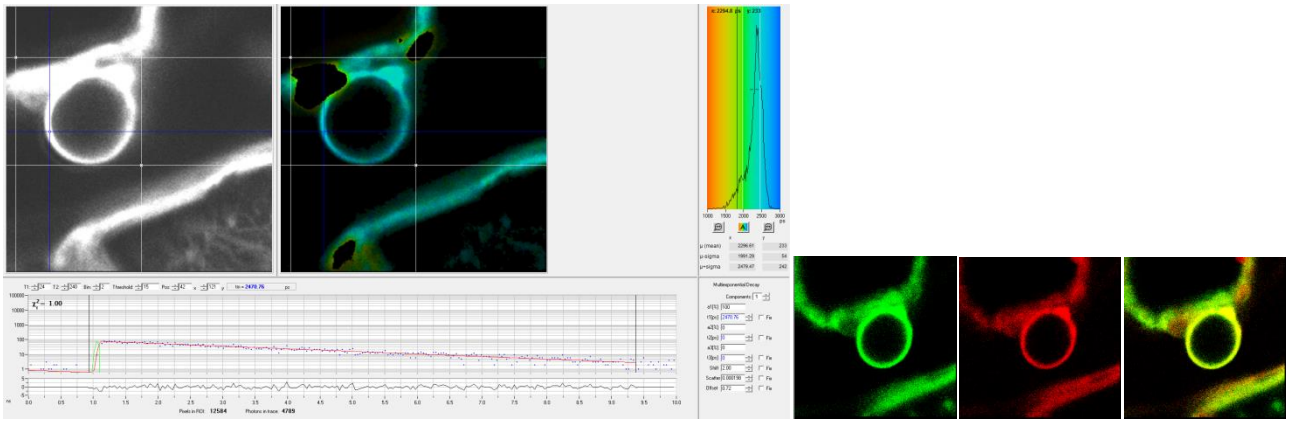

YUC9

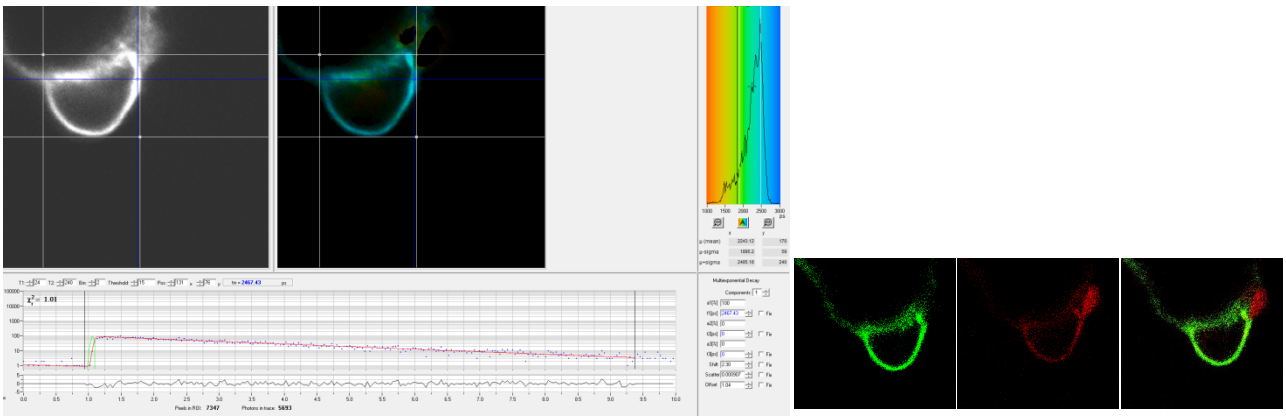

YUC11

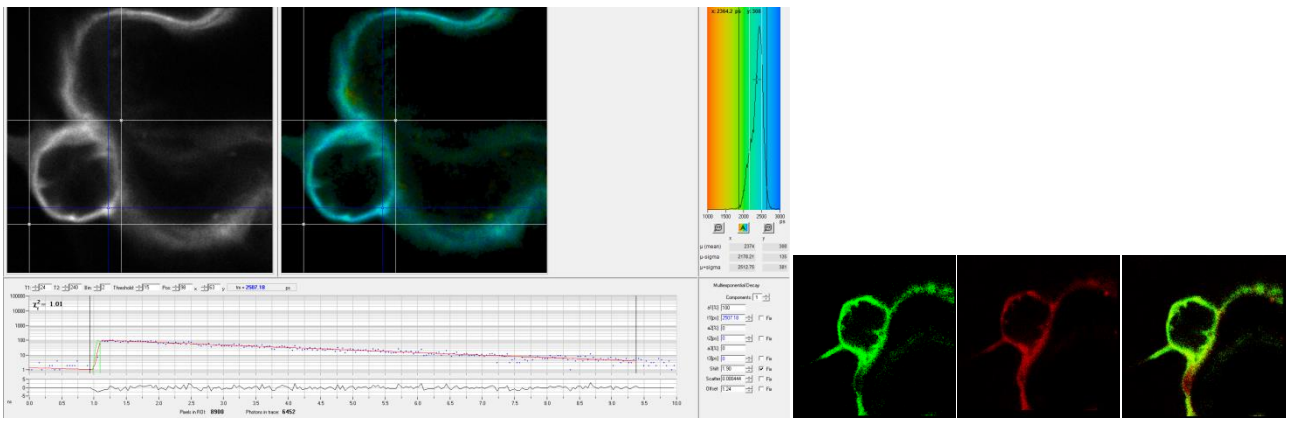

TAA1

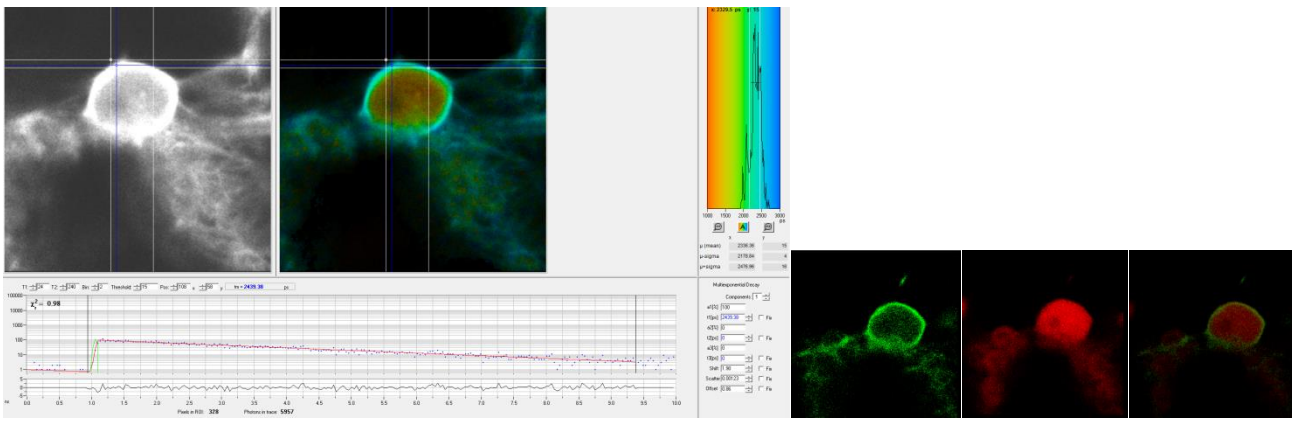

Supplementary Figure S4